# Critical Role for Isoprenoids in Apicoplast Biogenesis by Malaria Parasites

**Megan Okada[1], Krithika Rajaram[2], Russell P. Swift[2], Amanda Mixon[1], John Alan Maschek[3], Sean T. Prigge[2], Paul A. Sigala[1*]**

[1]Department of Biochemistry, University of Utah School of Medicine, Salt Lake City, Utah, United States; [2]Department of Molecular Microbiology and Immunology, Johns Hopkins School of Public Health, Baltimore, Maryland, United States; [3]Metabolomics Core, University of Utah Health Sciences Center, Salt Lake City, Utah, United States

[*]For correspondence: p.sigala@biochem.utah.edu

## ABSTRACT

Isopentenyl pyrophosphate (IPP) is an essential metabolic output of the apicoplast organelle in *Plasmodium falciparum* malaria parasites and is required for prenylation-dependent vesicular trafficking and other cellular processes. We have elucidated a critical and previously uncharacterized role for IPP in apicoplast biogenesis. Inhibiting IPP synthesis blocks apicoplast elongation and inheritance by daughter merozoites, and apicoplast biogenesis is rescued by exogenous IPP and polyprenols. Knockout of the only known isoprenoid-dependent apicoplast pathway, tRNA prenylation by MiaA, has no effect on blood-stage parasites and thus cannot explain apicoplast reliance on IPP. However, we have localized an annotated polyprenyl synthase (PPS) to the apicoplast lumen. PPS knockdown is lethal to parasites, rescued by IPP, and blocks apicoplast biogenesis, thus explaining apicoplast dependence on isoprenoid synthesis. We hypothesize that PPS synthesizes long-chain polyprenols critical for apicoplast membrane fluidity and biogenesis. This work critically expands the paradigm for isoprenoid utilization in malaria parasites and identifies a novel essential branch of apicoplast metabolism suitable for therapeutic targeting.

**INTRODUCTION:** *Plasmodium falciparum* malaria parasites are single-celled eukaryotes that harbor a non-photosynthetic plastid organelle called the apicoplast which houses core metabolic pathways and is essential for parasite viability.[1] Because human cells lack this organelle and many of its constituent enzymes, the apicoplast has been viewed as a potentially rich source of new parasite-specific drug targets. However, cashing in on this potential has proved challenging, since many apicoplast pathways, including heme[2, 3] and fatty acid synthesis[4, 5], are dispensable during parasite infection of erythrocytes when all malaria symptoms arise. Multiple antibiotics, including doxycycline and clindamycin, block apicoplast biogenesis and inheritance and kill parasites, but their slow activity over several lifecycles has been a fundamental limitation to broad clinical application.[6]

A key, essential function of the apicoplast is biosynthesis and export of the isomeric isoprenoid precursors, isopentenyl pyrophosphate (IPP) and dimethylallyl pyrophosphate (DMAPP), via the non-mevalonate/methylerythritol phosphate (MEP) pathway. IPP and DMAPP, which can be interconverted by an IPP isomerase, are critical for diverse cellular processes that include prenylation of proteins involved in vesicular trafficking, dolichol-mediated protein glycosylation, and biosynthesis of mitochondrial ubiquinone and heme A.[7-10] Indeed, exogenous IPP is able to rescue parasites from lethal apicoplast dysfunction or disruption, highlighting the essential requirement for this isoprenoid precursor outside the apicoplast in blood-stage parasites.[11] Consistent with these critical cellular roles for IPP, the MEP pathway inhibitor fosmidomycin (FOS) kills parasites in the first lifecycle of treatment.[8, 11, 12] This first-cycle FOS activity contrasts with the delayed, second-cycle death observed for *Plasmodium* parasites treated with antibiotics such as doxycycline and clindamycin that are thought to block translation of the 35-kb apicoplast genome and the predominantly organelle-maintenance pathways it encodes. These contrasting

kinetics have led to a prevailing view in the literature that essential apicoplast functions can be segregated into two general categories: (1) anabolic pathways that produce metabolites required outside the apicoplast and whose inhibition causes first-cycle parasite death or (2) housekeeping pathways that are only required for organelle maintenance and whose inhibition causes delayed, second-cycle defects.[13-15] Although this simple paradigm has been useful for conceptualizing general apicoplast functions, exceptions to this model have been reported[12, 16-18] and thus its general validity remains uncertain.

Since exogenous IPP rescues parasites from lethal apicoplast disruption,[11] isoprenoid biosynthesis has been thought to only serve essential roles outside this organelle.[7, 12, 15, 16, 19-21] Indeed, *P. falciparum* expresses an essential cytoplasmic polyprenyl synthase (PF3D7_1128400) whose dual farnesyl/geranylgeranyl pyrophosphate synthase (FPPS/GGPPS) activity is critical for condensing isoprenoid precursors into longer polyprenyl-PP groups required for diverse cellular processes such as protein prenylation and dolichol synthesis.[19, 22, 23] In addition, known prenyltransferases, which attach prenyl groups such as FPP and GGPP to client proteins, are also cytoplasmic.[20]

In contrast to this prevailing paradigm, we have unraveled a novel essential arm of isoprenoid metabolism and utilization within the apicoplast and provide direct evidence that IPP and its condensation into downstream linear isoprenoids are required for apicoplast branching and inheritance by daughter merozoites. Genetic knockout of MiaA-dependent tRNA prenylation, the only previously predicted isoprenoid-dependent pathway in the apicoplast,[1] has no effect on blood-stage parasites, and thus MiaA cannot account for apicoplast dependence on IPP. However, we have localized a previously annotated polyprenyl synthase (PPS, PF3D7_0202700)[24] to the apicoplast lumen and show that its conditional knockdown is lethal to parasites, can be rescued by

IPP and long- but not short-chain polyprenols, and blocks apicoplast inheritance. We posit that this apicoplast PPS functions downstream of IPP synthesis to produce longer-chain isoprenoids essential for apicoplast membrane fluidity during organelle biogenesis. This discovery critically expands the paradigm for isoprenoid utilization in *P. falciparum*, identifies a potential new apicoplast drug target, and uncovers an organelle maintenance pathway whose inhibition causes first-cycle defects in apicoplast inheritance in contrast to delayed death-inducing antibiotics.

## RESULTS

**Apicoplast elongation and branching require isoprenoid precursor synthesis.** The *P. falciparum* literature has focused almost exclusively on the essential roles of isoprenoid metabolism outside the apicoplast.[7, 11, 14, 15, 19, 20] Nevertheless, several prior studies reported that MEP-pathway inhibitors such as FOS and MMV008138 blocked apicoplast elongation in lethally treated parasites, suggesting a possible role for IPP in apicoplast biogenesis.[25-27] These prior studies, however, could not rule out that defects in apicoplast development caused by MEP-pathway inhibitors were due to non-specific effects from the pleiotropic cellular dysfunctions inherent to parasite death.[19] We revisited FOS inhibition of apicoplast biogenesis to further test and distinguish specific versus non-specific effects on organelle development.

We first tested the effect of 10 μM FOS (10x $EC_{50}$) on apicoplast elongation in synchronized cultures of two different parasite strains: D10 parasites expressing the apicoplast-targeted acyl carrier protein (ACP) leader sequence fused to GFP ($ACP_L$-GFP)[28] and a recently published NF54 parasite line (PfMev) that expresses $ACP_L$-GFP as well as heterologous enzymes that enable cytoplasmic synthesis of IPP from exogenous mevalonate precursor, independent of the apicoplast MEP pathway.[29] Consistent with prior reports,[25-27, 30] we observed that synchronized

ring-stage parasites treated with FOS developed into multi-nuclear schizonts but failed to elongate the apicoplast, which retained a focal, unbranched morphology in PfMev (Figure 1A) and D10 parasites (Figure 1- figure supplements 1-3). Although MEP pathway activity is detectable in ring-stage parasites,[31, 32] identical inhibition of apicoplast elongation in schizonts was observed if FOS was added to trophozoites 12 hours after synchronization (Figure 1, A and C, and Figure 1- figure supplement 2), suggesting continued reliance on de novo synthesis. In contrast to FOS treatment, parasites treated with lethal doses (10-100x $EC_{50}$) of drugs that target processes outside the apicoplast, including DSM1 (mitochondrial dihydroorotate dehydrogenase inhibitor),[33] atovaquone (ATV, mitochondrial cytochrome b inhibitor),[34] blasticidin-S (Blast-S, cytoplasmic translation inhibitor),[35] or WR99210 (WR, cytoplasmic dihydrofolate reductase inhibitor),[36] exhibited normal apicoplast biogenesis as they developed into schizonts, very similar to untreated parasites (Figure 1, B and C, and Figure 1- figure supplement 2). These observations strongly suggest that defects in apicoplast elongation observed with FOS treatment are due to specific inhibition of MEP pathway activity rather than non-specific, secondary effects of parasite death.

Multiple studies have reported that FOS-treated parasites grow normally in the presence of exogenous IPP and do not show evidence of apicoplast loss,[11, 12, 21, 29] suggesting that IPP rescues apicoplast biogenesis from FOS-induced defects. To directly test this conclusion, we simultaneously treated synchronized rings with 10 µM FOS and either 200 µM IPP or 50 µM mevalonate (for PfMev parasites) and observed normal apicoplast elongation and branching in schizonts (Figure 1, A and C, and Figure 1- figure supplement 2), consistent with a prior report.[26] These observations directly support the conclusion that apicoplast elongation requires isoprenoid synthesis.

To further test this conclusion via genetic disruption rather than pharmacological inhibition, we utilized a previously reported line of PfMev parasites in which the apicoplast-targeted deoxyxylulose-5-phosphate synthase (DXS), the first enzyme in the MEP isoprenoid synthesis pathway, had been genetically deleted (ΔDXS).[37] These parasites require exogenous mevalonate to support cytoplasmic IPP synthesis, since they lack a functional apicoplast MEP pathway. In the presence of 50 μM mevalonate, ΔDXS parasites displayed normal apicoplast elongation and branching in schizonts. However, washing out mevalonate from ring-stage ΔDXS parasites to ablate IPP synthesis resulted in multinuclear schizonts with focal, unbranched apicoplast morphologies identical to those observed in the presence of FOS (Figure 1, D and E, and Figure 1- figure supplement 4). These results strongly support the conclusion that apicoplast elongation and branching require IPP synthesis.

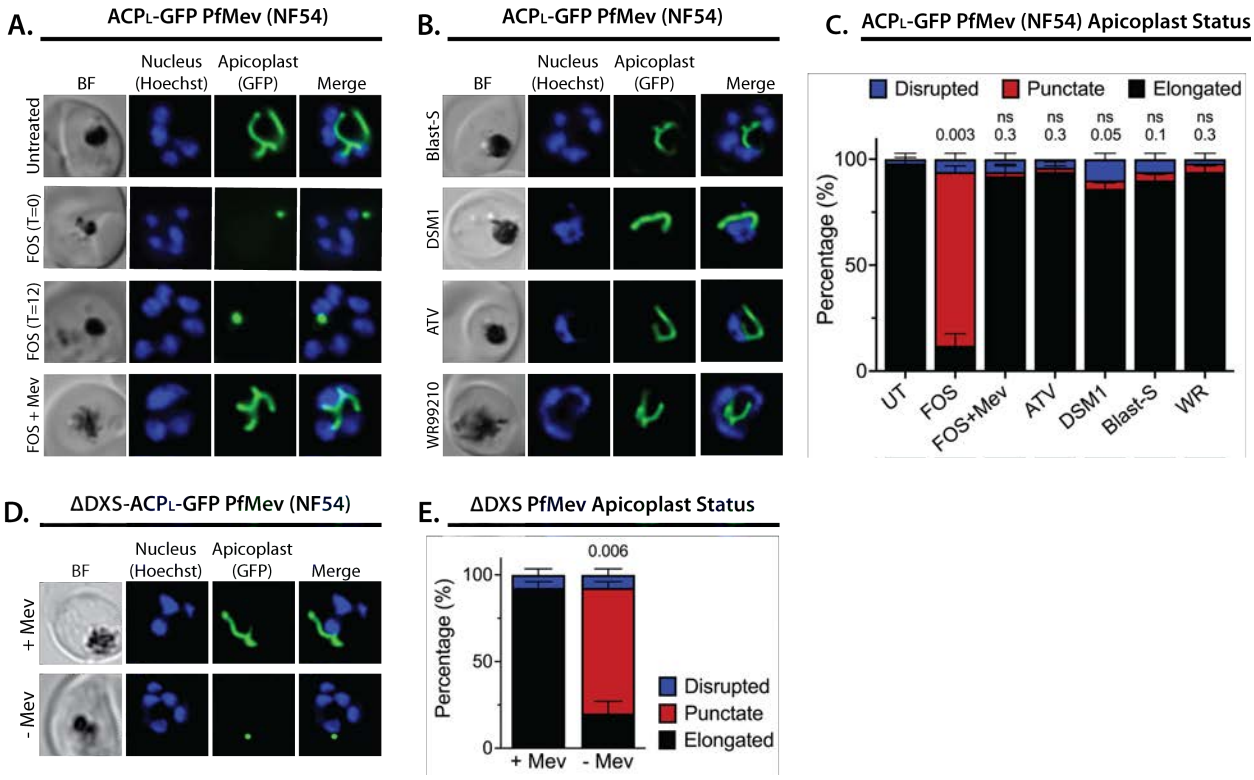


**Figure 1.** Inhibition of isoprenoid precursor biosynthesis specifically blocks apicoplast elongation and branching. Bright field (BF) and fluorescent microscopy images of live NF54 PfMev parasites that were **(A)** untreated or treated with 10 μM fosmidomycin (FOS) in the absence or presence of

50 μM DL-mevalonate (Mev), or **(B)** treated with 6 μM blasticidin-S (Blast-S), 2 μM DSM1, 100 nM atovaquone (ATV), or 5 nM WR99210. **(C)** Statistical analysis of apicoplast morphology for 50 total parasites imaged for each condition in panels A and B from two independent experiments. Apicoplast morphologies were scored as punctate (focal), elongated, or disrupted (dispersed); counted; and plotted by histogram as the fractional population with the indicated morphology. Error bars represent standard deviations from replicate experiments. Two-tailed unpaired t-test analysis was used to determine the significance of observed population differences compared to untreated (UT) parasites (P values given above each condition, ns = not significant). **(D)** Live-cell imaging of ΔDXS PfMev parasites in the presence or absence of 50 μM Mev. **(E)** Statistical analysis of parasites imaged in panel D and performed as in panel C. The P value is for comparison of apicoplast morphologies ±Mev conditions. In all experiments, synchronized ring-stage parasites were incubated with the indicated treatments for 36 hours prior to live-cell imaging. Parasite nuclei were visualized using 1 μg/ml Hoechst 33342. The parasite apicoplast was visualized using the $ACP_L$-GFP encoded by the PfMev line. Absolute parasite counts for all microscopy experiments are shown in Figure 1- Source Data 1.

**Figure supplement 1.** Additional epifluorescence images of PfMev NF54 parasites treated with FOS and other drugs.

**Figure supplement 2.** Epifluorescence images and analysis of D10 $ACP_L$-GFP parasites treated with FOS and other drugs.

**Figure supplement 3.** Additional epifluorescence images of D10 parasites treated with FOS and other drugs.

**Figure supplement 4.** Additional epifluorescence images of ΔDXS PfMev parasites cultured ±Mev.

**Source data 1.** Absolute parasite counts for all microscopy experiments.

**Inhibition of isoprenoid synthesis prevents apicoplast inheritance by daughter parasites.** To stringently test that IPP synthesis is required for apicoplast biogenesis, we next asked if FOS treatment prevented daughter parasites from inheriting the apicoplast, as predicted to occur if the apicoplast fails to elongate and divide in schizonts and as commonly observed for antibiotic inhibitors of apicoplast housekeeping pathways.[12, 38] Simultaneous treatment of ring-stage parasites with both FOS and IPP rescued growth defects and resulted in normal apicoplast elongation and division (Figure 1A and Figure 1- figure supplement 1), as expected since IPP is the direct anabolic product of the MEP pathway specifically inhibited by FOS. Thus, concomitant treatment with IPP and FOS cannot distinguish whether MEP pathway inhibition prevents

211 apicoplast inheritance by daughter parasites. To bypass this fundamental limitation, we devised
212 the following alternative strategy.

213 The apicoplast begins to elongate near the onset of schizogony before branching and then
214 dividing in late, segmenting schizonts.[28, 39] Despite manifesting defects in apicoplast elongation in
215 early schizogony, FOS-treated parasites continue to divide nuclear DNA and transition into mature
216 schizonts before stalling prior to segmentation into merozoites (Figure 1A).[30] This observation
217 suggested that defects in apicoplast biogenesis were not the immediate cause of parasite death in
218 the present cell cycle and that such defects preceded a broader essential requirement for IPP outside
219 the apicoplast in mature schizonts. Recent works suggest this broader essentiality to be IPP-
220 dependent protein prenylation.[15, 30] We therefore reasoned that if IPP supplementation were
221 delayed until mid-schizogony, after the onset of apicoplast elongation defects but before broader
222 cellular death, it might be possible to rescue parasite viability without rescuing apicoplast
223 biogenesis and thereby produce viable parasite progeny that lacked the intact apicoplast.

224 Synchronized ring-stage PfMev parasites were treated with 10 μM FOS for 48 hours, with
225 50 μM mevalonate added at 0, 30, 34, or 38 hours after synchronization. (Figure 2A). Parasites
226 were allowed to expand for three subsequent cycles in 50 μM mevalonate, with growth monitored
227 by flow cytometry. We observed a hierarchy of growth rescue by mevalonate, with full rescue
228 (relative to no FOS treatment) of parasites supplemented with mevalonate at 0 hours post-
229 synchronization and decreasing rescue for increasingly delayed supplementation at 30, 34, or 38
230 hours (Figure 2B), presumably due to fewer viable parasites surviving the initial cycle.

231 To assess and quantify apicoplast status in rescued parasites, we cloned out individual
232 parasites at 60 hours post-synchronization in the second growth cycle. Apicoplast status in the
233 resulting clones was determined by live parasite microscopy of organelle morphology, apicoplast

genome PCR, and growth ± mevalonate. Although FOS-treated parasites supplemented simultaneously with mevalonate showed no evidence for apicoplast loss in clonal progeny, a fraction of clonal parasites derived from delayed mevalonate rescue showed clear signs of apicoplast loss, including a dispersed apicoplast $ACP_L$-GFP signal, loss of the apicoplast genome, and growth dependence on exogenous mevalonate (Figure 2C and Figure 2- figure supplements 1–4). The fraction of clonal parasites with a disrupted apicoplast increased from 10% in parasites supplemented with mevalonate at 30 hours to over 80% in parasites supplemented at 38 hours (Figure 2D). These results provide direct evidence that inhibiting IPP synthesis alone is sufficient to block apicoplast biogenesis and prevent organelle inheritance by daughter parasites.

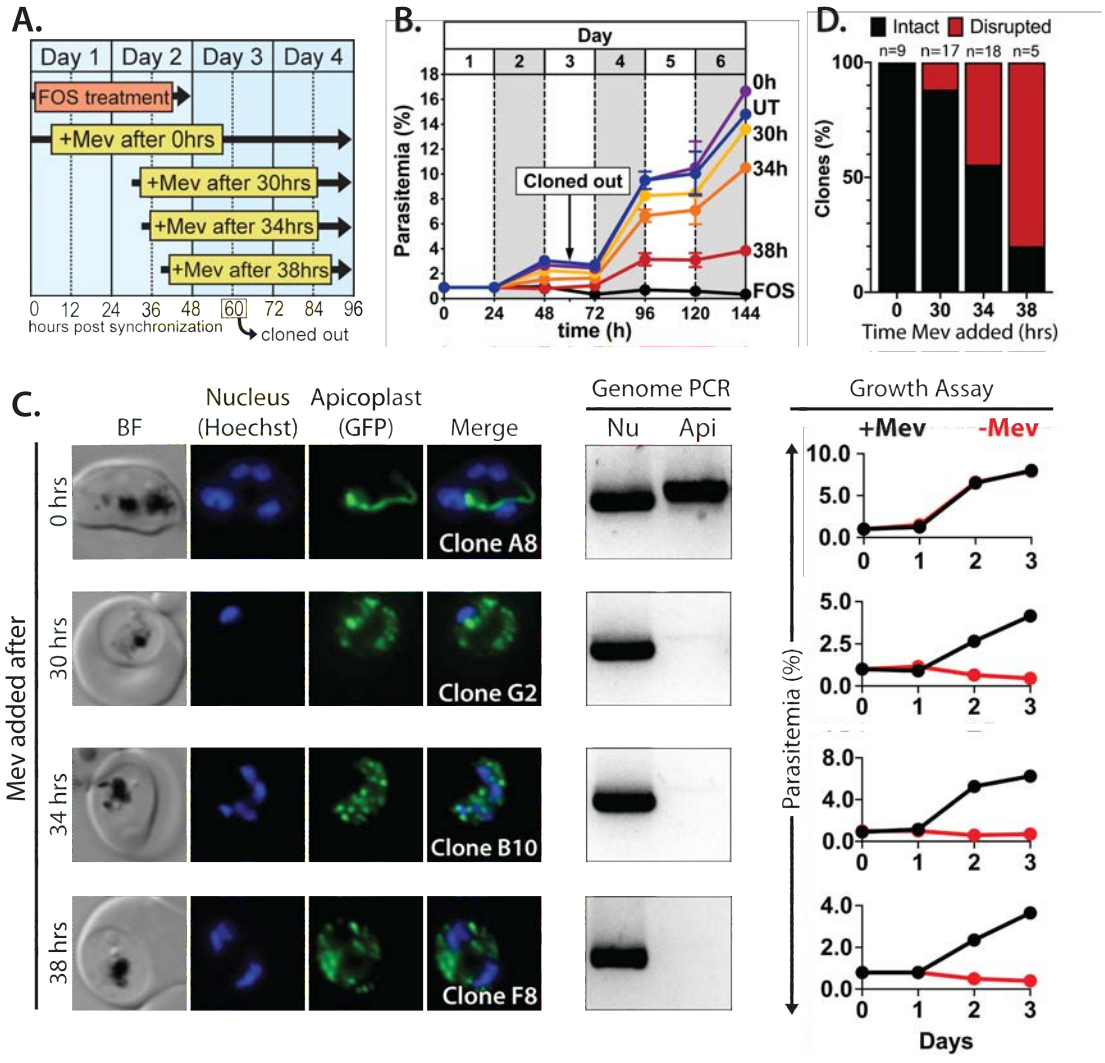

**Figure 2.** Inhibiting isoprenoid precursor biosynthesis prevents apicoplast inheritance by daughter parasites. **(A)** Schematic summary of delayed mevalonate rescue of fosmidomycin (FOS) treatment. PfMev parasites were synchronized with 5% D-sorbitol and cultured in 10 µM FOS (washed out after 48 hours in 2$^{nd}$-cycle rings) without or with addition of 50 µM DL-mevalonate (Mev) at 0, 30, 34, or 38 hours after synchronization. Clonal parasites from all growth conditions were isolated at 60 hours post-synchronization by limiting dilution and growth in 50 µM Mev. **(B)** Parasite growth was monitored for 6 days by flow cytometry using acridine orange staining (FOS = treated only with FOS, UT = untreated, 0h – 38h time delay of Mev addition after synchronization and initiation of FOS treatment). **(C)** Bright-field (BF) and fluorescence microscopy images of live clonal parasites isolated after 60 hours of growth under the conditions described in panel A. Parasite nuclei were visualized using 1 µg/ml Hoechst 33342. To the right of each clonal image panel is a gel image showing the result of PCR analysis to amplify a (Nu) nuclear (PPS, PF3D7_0202700) and (Api) apicoplast (SufB, PF3D7_API04700) gene and a growth assay to monitor the ability of each isolated clone in the presence or absence of 50 µM Mev. Data points are the average of two technical replicates from a single growth assay. Error bars (stdev) are smaller than the data points. **(D)** Graphical representation of the number of clones isolated under each growth condition and the clonal percentage with an intact or disrupted apicoplast (determined by microscope analysis of $ACP_L$-GFP signal and genomic PCR).

**Figure supplement 1.** Epifluorescence microscopy images of clonal parasites isolated after FOS treatment and rescue by mevalonate addition at 0 hours after synchronization.

**Figure supplement 2.** Epifluorescence microscopy images of clonal parasites isolated after FOS treatment and rescue by mevalonate addition at 30 hours after synchronization. Clone headers for parasites with a disrupted apicoplast are yellow.

**Figure supplement 3.** Epifluorescence microscopy images of clonal parasites isolated after FOS treatment and rescue by mevalonate addition at 34 hours after synchronization. Clone headers for parasites with a disrupted apicoplast are yellow.

**Figure supplement 4.** Epifluorescence microscopy images of clonal parasites isolated after FOS treatment and rescue by mevalonate addition at 38 hours after synchronization. Clone headers for parasites with a disrupted apicoplast are yellow.

## The MiaA pathway for apicoplast tRNA prenylation is dispensable for blood-stage parasites.

Why do apicoplast elongation and branching require IPP synthesis? Currently, the only predicted isoprenoid-dependent metabolic pathway in the apicoplast is tRNA prenylation by MiaA,[1, 20] which catalyzes the attachment of a dimethylallyl group to the $N^6$ moiety of adenine at position 37 of certain tRNAs.[40] DMAPP is produced in tandem with IPP in the terminal enzymatic step of the MEP pathway and can be interconverted with IPP by an IPP/DMAPP isomerase.[7, 11] Prenylation of A37 is often accompanied by methylthiolation by the radical SAM enzyme, MiaB.[41] Although

282 genes encoding MiaA (PF3D7_1207600) and MiaB (PF3D7_0622200) are annotated in the *P.*
283 *falciparum* genome and MiaA protein has been detected by mass spectrometry in the apicoplast-
284 specific proteome,[42] neither protein has been directly studied in parasites. Nevertheless, both
285 proteins are predicted to be non-essential for blood-stage *Plasmodium* based on genome-wide
286 knockout (KO) studies in *P. berghei*[43] and *P. falciparum*.[44]

287 To directly test whether MiaA function is essential for *P. falciparum* parasites and can
288 account for apicoplast dependence on isoprenoid synthesis, we used CRISPR/Cas9 to target MiaA
289 for gene disruption by double-crossover homologous recombination (Figure 3- figure supplement
290 1). PfMev parasites were transfected and selected in the presence of 50 μM mevalonate to ensure
291 that parasites would remain viable even if deletion of MiaA resulted in apicoplast disruption.
292 Parasites that had integrated the knock-out plasmid returned from transfection, and loss of the
293 MiaA gene was confirmed by genomic PCR (Figure 3- figure supplement 1). The ΔMiaA parasites
294 grew equally well in the presence or absence of mevalonate and grew indistinguishably from the
295 parental PfMev parasites (Figure 3A). The presence of an intact apicoplast was confirmed by
296 genomic PCR analysis and live parasite microscopy (Figure 3B and Figure 3- figure supplement
297 1). These results indicate that MiaA is dispensable for blood-stage parasites and that deletion of
298 this gene does not affect apicoplast biogenesis. Therefore, loss of function of MiaA, the only
299 predicted isoprenoid-dependent pathway in the apicoplast, cannot account for apicoplast
300 dependence on IPP synthesis, suggesting an alternative role for IPP in organelle elongation.

301

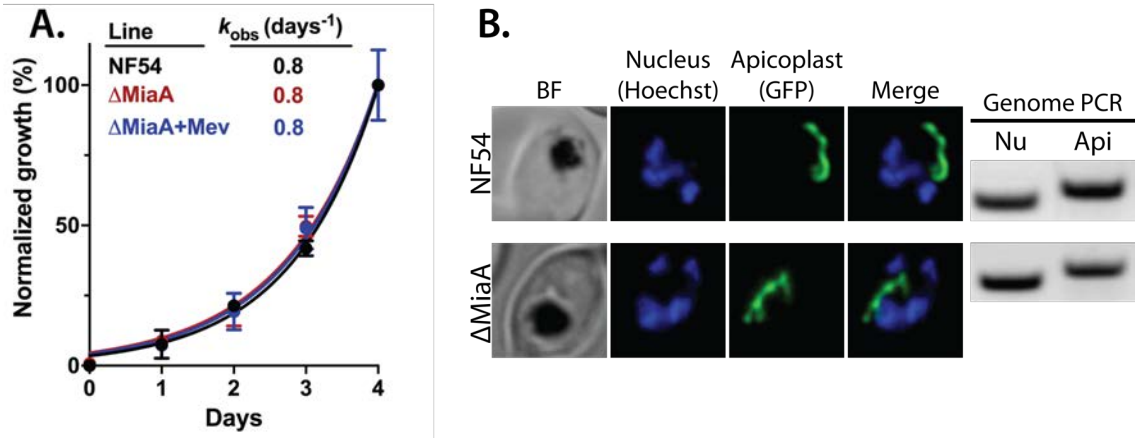


**Figure 3.** Genetic disruption of MiaA has no effect on parasite growth or apicoplast biogenesis. **(A)** Growth analysis indicates that parental PfMev NF54 parasites and ΔMiaA parasites cultured in the absence or presence of 50 μM Mev grow indistinguishably with identical rate constants ($k_{obs}$) for asynchronous culture expansion. Parasitemia values for each sample are the average ±SD of three biological replicates and were normalized to the parasitemia on day 4 and fit with an exponential growth model. **(B)** Live-parasite imaging and genomic PCR analysis indicate normal apicoplast morphology and retention of the apicoplast genome in parental PfMev and ΔMiaA parasites. BF = brightfield, Nu = nuclear gene (LDH, PF3D7_1324900), and Api = apicoplast gene (SufB, PF3D7_API04700).

**Figure supplement 1.** PCR genotyping of PfMev ΔMiaA parasites and additional epifluorescence images of apicoplast morphology.

**Apicoplast biogenesis requires polyprenyl isoprenoid synthesis.** Except for MiaA-catalyzed tRNA prenylation, all proposed roles for isoprenoids in *Plasmodium* parasites require head-to-tail condensation of DMAPP (5 carbons) and one or more IPP subunits (5 carbons) to form longer-chain isoprenoids, starting with formation of geranyl pyrophosphate (GPP, 10 carbons), farnesyl pyrophosphate (FPP, 15 carbons), and geranylgeranyl pyrophosphate (GGPP, 20 carbons).[7, 20] Recent studies reported that 5 μM geranylgeraniol (GGOH, the alcohol precursor of GGPP) can provide short-term (~1 cycle) rescue of parasite death due to treatment with FOS or indolmycin, an apicoplast tryptophan tRNA synthetase inhibitor.[15, 30] Based on these reports, we hypothesized that the dependence of apicoplast biogenesis on IPP might reflect a requirement for longer-chain

isoprenoids such that farnesol (FOH), GGOH, and/or longer-chain polyprenols might rescue the apicoplast branching defects caused by 10 μM FOS.

We treated synchronized NF54 and D10 parasites with both 10 μM FOS and 5 μM of either FOH or GGOH. Consistent with prior reports, 5 μM GGOH but not FOH partially rescued parasite growth from inhibition by FOS and enabled culture expansion into a second growth cycle (Figure 4- figure supplement 1). Nevertheless, both GGOH and FOH rescued apicoplast elongation and branching defects in schizonts when added simultaneously with FOS to synchronized rings (Figure 4 and Figure 4- figure supplements 2 and 3). Rescue of apicoplast branching by FOH and GGOH strongly suggests that apicoplast biogenesis depends on utilization of polyprenyl isoprenoids of three or more isoprene units. We extended these rescue experiments to include 5 μM decaprenol (50 carbons) and also observed rescue of apicoplast branching from FOS-induced defects. However, 5 μM β-carotene, which is a nonlinear carotenoid hydrocarbon derived from 8 prenyl groups (40 carbons), did not rescue apicoplast biogenesis from inhibition by FOS (Figure 4 and Figure 4- figure supplements 2 and 3). These results directly suggest that apicoplast biogenesis specifically requires synthesis of linear polyprenols containing three or more prenyl groups.

Iterative condensation of DMAPP with IPP subunits to form FPP, GGPP, and longer polyprenyl-PPs requires the function of a polyprenyl synthase. This family of enzymes uses a conserved dyad of DDXXD residues positioned near the protein surface of the active site binding pocket to coordinate $Mg^{2+}$ ions that bind the pyrophosphate headgroup of DMAPP, GPP, or FPP and position its allylic head relative to the vinyl tail of the IPP subunit.[45] Condensation of the two substrates via electrophilic alkylation elongates the nascent isoprenoid chain into the protein interior. Two amino acids just upstream of the first DDXXD motif determine the length of the resulting prenyl chain by forming a hydrophobic "floor" that gates the depth of the protein interior.

Indeed, dedicated FPPS enzymes feature an amino acid floor comprised of sequential Phe-Phe residues just upstream of the first DDXXD motif that sterically block synthesis of products longer than FPP.[46, 47] Sequence variations that replace just the more N-terminal Phe or both Phe-Phe groups with smaller residues (e.g., Ala or Ser) open up and extend the binding pocket and enable synthesis of GGPP or longer polyprenyl-PPs up to 14 isoprene units, respectively (Figure 5).[48]

A BLAST search of the *P. falciparum* genome with the sequence of the well-studied chicken FPP synthase (Uniprot P08836) reveals two parasite orthologs (PF3D7_1128400 and PF3D7_0202700) that retain the DDXXD dyads and other conserved sequence features expected of a polyprenyl synthase (Figure 5A and Figure 5- figure supplement 1). The best studied of these synthases is the cytosolic enzyme, PF3D7_1128400, which shares 34% sequence identity with avian FPPS and has been reported to catalyze formation of both FPP and GGPP.[22, 49, 50] Consistent with its ability to synthesize GGPP as the terminal product, PF3D7_1128400 has sequential Ser-Phe residues just upstream of the first DDXXD motif (Figure 5A).[49, 50] This cytoplasmic enzyme is reported to be essential based on inhibitor[19, 23] and gene-disruption studies in *P. berghei*[43] and *P. falciparum*[44] and is thought to synthesize the FPP and GGPP required for broad parasite isoprenoid metabolism, including protein prenylation and synthesis of dolichols, ubiquinone, and heme A.[7, 20]

We first considered the model that this cytoplasmic FPPS/GGPPS might have an essential role in producing GGPP required for apicoplast biogenesis. A recent study, however, identified a specific inhibitor (MMV019313) of PF3D7_1128400 that is lethal to parasites but does not impact apicoplast biogenesis.[19] We independently confirmed that lethal treatment with MMV019313 did not affect apicoplast branching in the PfMev line (Figure 5- figure supplement 2). These observations strongly suggest that the cytosolic FPPS/GGPPS is not the origin of the polyprenyl

synthase activity required for apicoplast biogenesis. Therefore, we turned our attention to the second isoprenoid synthase homolog in *P. falciparum*, PF3D7_0202700, which shares 23% sequence identity with avian FPPS.

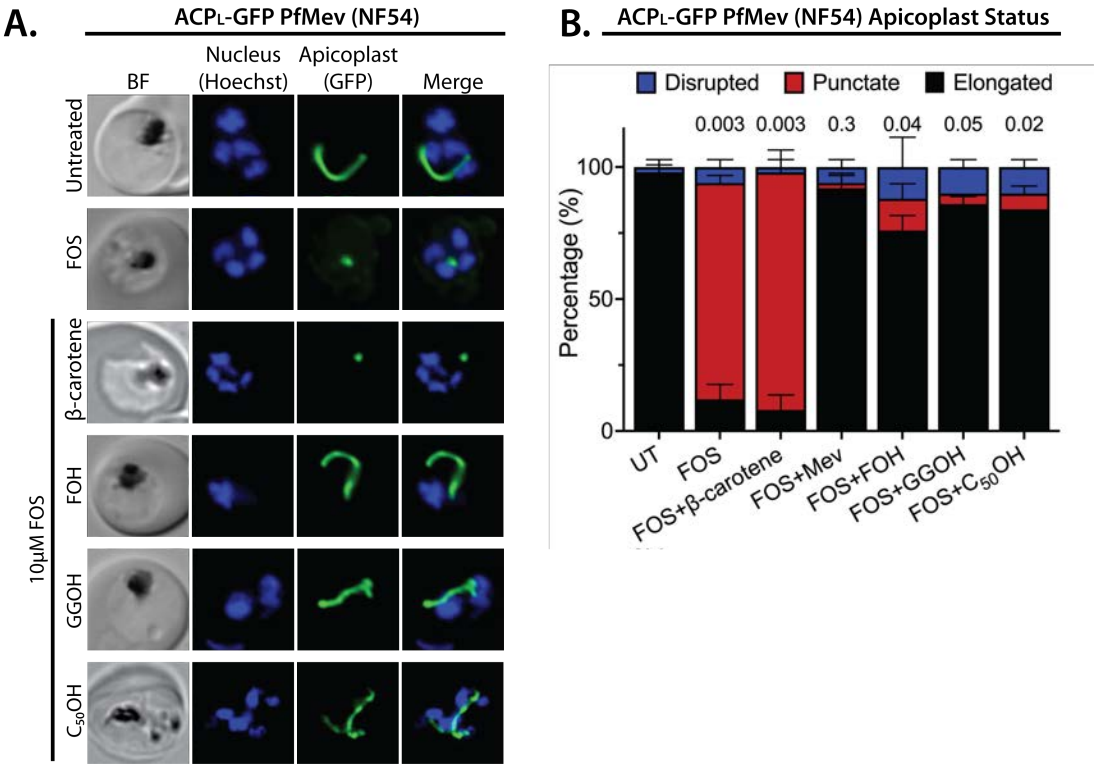


**Figure 4.** Apicoplast biogenesis requires linear polyprenyl isoprenoid synthesis. **(A)** 5 μM farnesol (FOH), geranylgeraniol (GGOH), or decaprenol ($C_{50}$-OH), but not β-carotene rescues apicoplast biogenesis from inhibition by 10 μM FOS in PfMev parasites. Synchronized ring-stage parasites were incubated with the indicated treatments for 36 hours and imaged by brightfield (BF) or fluorescence microscopy, with visualization of parasite nuclei by Hoechst staining and the apicoplast by $ACP_L$-GFP signal. **(B)** Statistical analysis of apicoplast morphology for 50 total parasites imaged for each condition in panel A from two independent experiments. Apicoplast morphologies were scored as punctate (focal), elongated, or disrupted (dispersed); counted; and plotted by histogram as the fractional population with the indicated morphology. Error bars represent standard deviations from replicate experiments. Two-tailed unpaired t-test analysis was used to determine the significance of observed population differences compared to untreated (UT) parasites (P values given above each condition, ns = not significant).

**Figure supplement 1.** 5 μM GGOH but not FOH partially rescues parasite growth from inhibition by 10 μM FOS in continuous-growth assays with PfMev parasites.

**Figure supplement 2.** Additional epifluorescence microscopy images of PfMev parasites treated with FOS and FOH, GGOH, $C_{50}$-OH, or β-carotene.

**Figure supplement 3.** Epifluorescence microscopy images of D10 $ACP_L$-GFP parasites treated with FOS and FOH, GGOH, $C_{50}$-OH, or β-carotene.

**Localization of an annotated polyprenyl synthase to the apicoplast.** Like the cytoplasmic FPP/GGPP synthase, PF3D7_0202700 retains the DDXXD sequence dyad expected for a polyprenyl pyrophosphate synthase. In addition, the amino acid floor of PF3D7_0202700 features a sterically smaller Gly-Ser dyad upstream of the first DDXXD (Figure 5A and figure 5- figure supplement 1) that suggests an ability to synthesize longer-chain isoprenoids greater than four isoprene units. Consistent with these features, sequence similarity searches via NCBI BLAST[51] and MPI HHpred[52] identify polyprenyl synthase homologs from bacteria, algae, and plants that share ~30% sequence identity with PF3D7_0202700 and have annotated functions in synthesizing polyprenyl isoprenoids of 4 – 10 units (Figure 5- figure supplement 3). Using *E. coli* octaprenyl pyrophosphate synthase (PDB 3WJK, 28% identity) as template, we generated a homology model of PF3D7_0202700 to visualize the possible structure of its active site (Figure 5B).

A prior in vitro study of PF3D7_0202700 function, using truncated recombinant protein expressed in *E. coli* or impure parasite extracts, reported an ability to synthesize polyprenyl-PP products of 8 – 11 isoprene units.[24] Based on the authors' description, this truncated recombinant protein appears to have lacked one of the DDXXD motifs. Because of this difference from the native protein and the impurity of the parasite-derived protein, it remains possible that the native, pure protein has a distinct product spectrum than previously reported. Nevertheless, this in vitro activity and the general sequence features of PF3D7_0202700 support its function as a long-chain polyprenyl synthase (PPS).

Prior immunofluorescence studies of this PPS, using a polyclonal antibody raised against the truncated recombinant protein, were unable to localize PF3D7_0202700 to a specific sub-

417 cellular compartment.[53] Analysis of the protein sequence with PlasmoAP[54] suggested the presence
418 of a subcellular-targeting leader sequence, with strong prediction of an apicoplast-targeting transit
419 peptide but uncertainty in the presence of a signal peptide. To localize PPS within parasites, we
420 engineered Dd2 *P. falciparum* lines to episomally express full-length PPS fused to either C-
421 terminal GFP or RFP. In live parasites, focal PPS-GFP fluorescence was detected in a tubular
422 compartment proximal to but distinct from the mitochondrion, as expected for apicoplast
423 localization. Additional immunofluorescence analysis of the PPS-GFP line revealed strong co-
424 localization between PPS-GFP and the apicoplast acyl carrier protein (ACP) (Figure 5C and Figure
425 5- figure supplement 4).

426 To further confirm apicoplast targeting of PPS, we stably disrupted the apicoplast in the
427 PPS-GFP Dd2 line by culturing these parasites in 2 μM doxycycline and 200 μM IPP for one
428 week.[11, 55] As expected for an apicoplast-targeted protein, the PPS-GFP signal in these parasites
429 displayed a constellation of dispersed fluorescent foci, rather than the concentrated signal observed
430 in untreated parasites (Figure 5D and Figure 5- figure supplement 4). Western blot analysis of the
431 PPS-RFP parasites revealed two bands at the expected molecular weight of the full-length protein
432 and a smaller, proteolytically processed form, consistent with import into the apicoplast lumen
433 (Figure 5E).[28] In the apicoplast-disrupted parasites, however, only a single PPS-RFP band at the
434 size of the full-length protein was detected, as expected for loss of apicoplast import and lack of
435 protein processing.[11, 38] On the basis of these observations, we conclude that PF3D7_0202700 is
436 an apicoplast-targeted PPS. This localization, the predicted ability of this enzyme to synthesize
437 polyprenyl PPs longer than 4 isoprenes, and our observation that decaprenol rescued FOS-induced
438 defects in apicoplast biogenesis all suggested a critical role for this protein in apicoplast
439 maintenance.

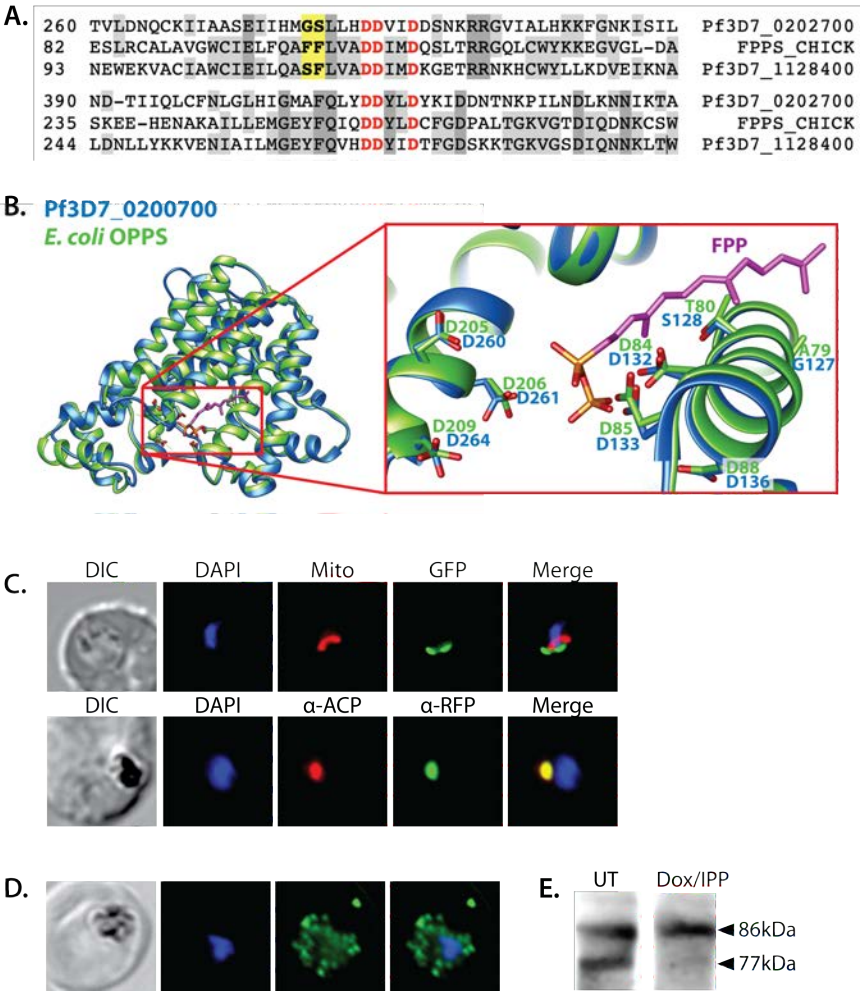


**Figure 5.** Sequence alignment and localization of the polyprenyl synthase (PPS) PF3D7_0202700 to the apicoplast. **(A)** Focal sequence alignment of avian farnesyl pyrophosphate synthase (FPPS, Uniprot P08836) with its two *P. falciparum* homologs reveals the presence of conserved metal-binding DDXXD motifs (red) expected for polyprenyl synthase activity and chain-length determination residues (yellow) upstream of the first DDXXD. **(B)** Homology model of PF3D7_0202700 using *E. coli* octaprenyl pyrophosphate synthase (PDB 3WJK) as a structural template. The inset box is an enlargement of the active-site pocket showing the conserved Asp residues, bound FPP substrate, and product length-determining residues just upstream of the first DDXXD motif. **(C)** Brightfield (BF), fluorescence images (top) of live parasites episomally expressing PPS-GFP and stained with 10 nM Mitotracker Red and (bottom) immunofluorescence analysis (IFA) images of fixed parasites episomally expressing PPS-RFP stained with anti-RFP and anti-apicoplast ACP antibodies. **(D)** IFA images of fixed parasites expressing PPS-RFP that had been treated for >7 days with 2 µM doxycycline (Dox) and 200 µM IPP (to stably induce apicoplast loss) and stained with anti-RFP antibody to visualize PPS distribution. **(E)** Western blot analysis of untreated (UT) or Dox/IPP-treated parasites episomally expressing PPS-RFP. PPS-RFP expression was visualized using an anti-RFP antibody. The full western blot image is included in Figure 5- Source Data 1.

**Figure supplement 1.** Full sequence alignment of PF3D7_0202700, PF3D7_1128400, and avian FPPS (Uniprot P08836).

**Figure supplement 2.** Epifluorescence microscopy images and statistical analysis of PfMev and D10 parasites treated with 10 μM MMV091313.

**Figure supplement 3.** Results of sequence-similarity searches for PF3D7_0202700 using NCBI BLAST and MPI HHpred.

**Figure supplement 4.** Additional epifluorescence microscopy images of Dd2 parasite episomally expressing PPS-GFP or PPS-RFP.

**Source data 1.** Uncropped western blot image detecting PPS-RFP expression in parasites.

**PPS is essential for parasite viability and apicoplast biogenesis.** The genomic locus for PF3D7_0202700 was reported to be refractory to disruption in recent genome-wide KO studies in *P. berghei*[43] and *P.* falciparum,[44] suggesting an essential function. To directly test its functional essentiality in *P. falciparum*, we used CRISPR/Cas9[56] to tag the endogenous gene in Dd2 parasites to encode a C-terminal hemagglutinin (HA)-FLAG epitope fusion and the aptamer/TetR-DOZI system[57] that enables ligand-dependent regulation of protein expression using the non-toxic small molecule, anhydrotetracycline (aTc). In this system, normal protein expression occurs +aTc and translational repression is induced upon aTc washout (Figure 6A). Correct integration into the genomic locus with the expected genotype in both polyclonal and clonal parasites was confirmed by Southern blot (Figure 6- figure supplement 1). Expression of the ~60 kDa HA-FLAG-tagged, endogenous mature protein was detected by western blot (Figure 6B).

To test PPS essentiality for blood-stage parasite growth, we synchronized PPS knockdown (KD) parasites and monitored their growth ±aTc over multiple intraerythrocytic lifecycles. Because of inconsistency in detecting the endogenous PPS by western blot (WB), possibly due to low protein expression, we monitored PPS transcript levels by RT-qPCR in lieu of WB analysis. We observed robust knockdown of PPS mRNA levels by the second intraerythrocytic cycle (Figure 6C). The fate of target mRNA in the aptamer/TetR-DOZI system has not been

characterized in depth. Our data is consistent with a prior report[58] and suggests that TetR-DOZI binding after aTc washout leads to mRNA transcript degradation, possibly within stress granules targeted by DOZI-bound transcripts.[57] In the presence of aTc, culture parasitemia expanded in a step-wise fashion over the ~10 days of the growth assay such that the culture needed to be split multiple times to avoid over-growth (Figure 6C). Without aTc, however, the culture grew normally over the first 3 intraerythrocytic cycles but showed a major growth defect in the fourth cycle consistent with extensive parasite death observed by blood smear (Figure 6C and Figure 6- figure supplements 1 and 2). Parasite growth under -aTc conditions was rescued in the presence of 200 μM exogenous IPP (Figure 6C), indicating an essential PPS function within the apicoplast.

To test a role for PPS in synthesizing polyprenyl PP groups, we attempted to rescue parasite growth in -aTc conditions by adding 5 μM FOH, GGOH, or decaprenol. We observed that only decaprenol, but not FOH or GGOH, rescued parasite growth -aTc, and the magnitude of rescue by decaprenol was comparable to IPP (Figure 6C and Figure 6- figure supplement 2). These observations strongly suggest that PPS has an essential function downstream of IPP synthesis in converting isoprenoid precursors into longer-chain linear polyprenyl-PPs containing at least 5-10 isoprene units.

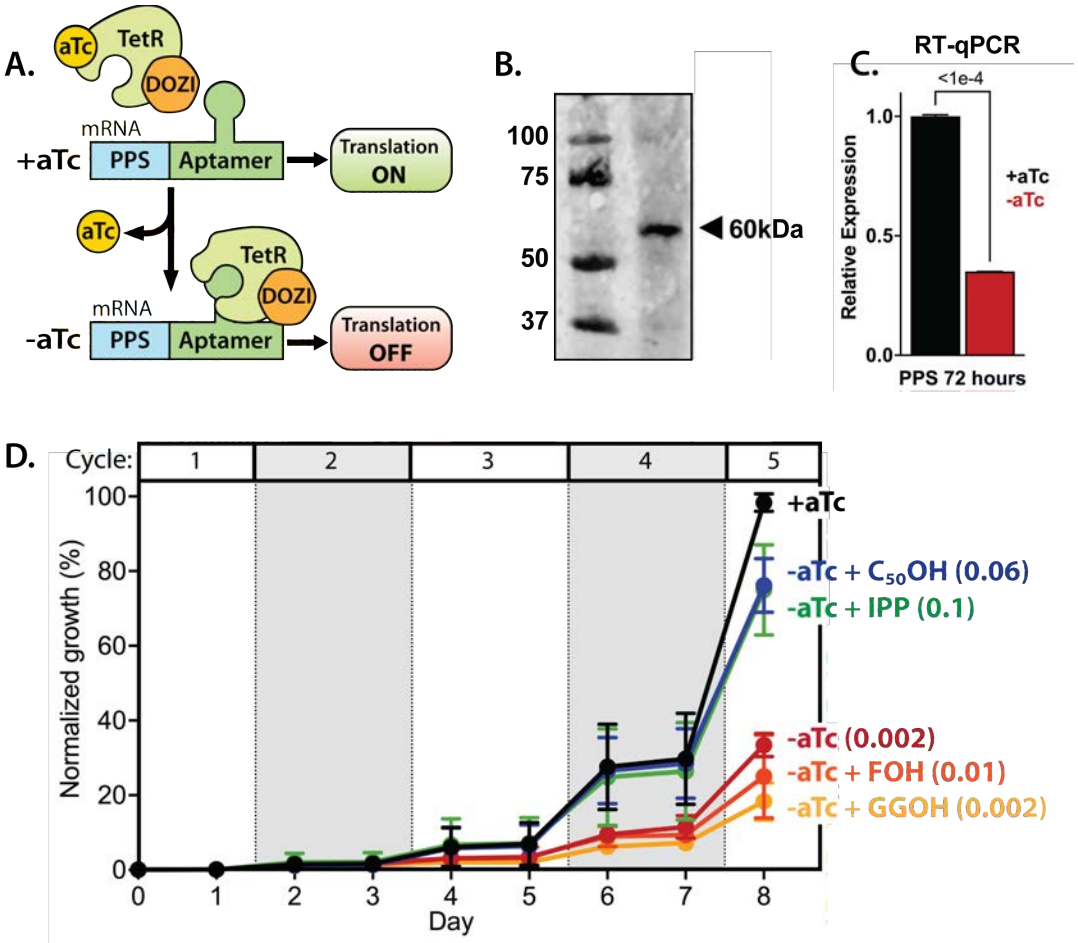


**Figure 6.** PPS (PF3D7_0202700) is essential for parasite viability and apicoplast function. **(A)** Schematic depiction of the aptamer/TetR-DOZI system for ligand-dependent protein expression. The target protein (PPS) is translated normally in the presence of anhydrotetracycline (aTc) but its translation is repressed without aTc. **(B)** Western blot of endogenously tagged PPS-HA/FLAG and probed with anti-HA epitope antibody showing detection of tagged PPS at the expected size for mature PPS of ~60 kDa. **(C)** RT-qPCR analysis of PPS transcript levels (normalized to the average of two nuclear control genes) in synchronous parasites cultured for 72 hours ±aTc. Significance of the observed difference was evaluated by two-tailed unpaired t-test with the indicated P value. **(D)** Synchronous growth assay of Dd2 parasites tagged at the PPS locus with the aptamer/TetR-DOZI system and grown ±aTc and ± 200 µM IPP or 5 µM farnesol (FOH), geranylgeraniol (GGOH), or decaprenol ($C_{50}$-OH). Parasitemia values for each condition are the average ±SD of two biological replicates. Two-tailed unpaired t-test analysis was used to determine the significance of observed parasitemia differences on day 8 for each condition compared to parasites cultured +aTc (P values given in parentheses).

**Figure supplement 1.** Scheme for modification of the PPS genomic locus to integrate the aptamer/TetR-DOZI system and Southern blot confirming correct integration.

**Figure supplement 2.** Blood-smear images of Dd2 parasites tagged at the PPS locus with the aptamer/TetR-DOZI system and grown ±aTc for 8 days.

To test if PPS function is required for apicoplast biogenesis, we cultured PPS KD parasites in +aTc or -aTc/+IPP conditions for 12 days and then assessed apicoplast morphology in fixed parasites by αACP immunofluorescence. We reasoned that IPP would rescue parasite viability upon PPS KD but not interfere with assessing any defect in apicoplast biogenesis if IPP synthesis is upstream of PPS function. Immunofluorescence analysis (IFA) revealed that ~30% of parasites cultured in -aTc conditions had a dispersed ACP signal indicative of apicoplast disruption (Figure 7- figure supplement 1). Although this observation supports a critical role for PPS in apicoplast biogenesis, we wondered why PPS KD did not result in a higher fraction of parasites with disrupted apicoplast. We hypothesized that residual PPS expression resulting from incomplete KD combined with high IPP levels due to culture supplementation and endogenous MEP pathway activity might enable sufficient synthesis of polyprenols to attenuate the impact of PPS KD on apicoplast biogenesis.

To test this hypothesis and the contribution of MEP activity to the observed phenotype, we synchronized parasites to the ring stage and cultured them in ±aTc conditions for 96 hours (two 48-hour growth cycles) to knock down PPS expression before adding FOS and IPP at the start of the third growth cycle (Figure 7A). In this experiment, FOS was expected to inhibit endogenous MEP pathway activity without impacting apicoplast biogenesis since it was added concurrently with IPP, which fully rescues parasites from growth and apicoplast defects induced by FOS (Figure 1).[11, 21] We first used IFA to assess apicoplast morphology in schizonts at the end of the third growth cycle (38 hours after adding FOS and IPP). We observed normal apicoplast elongation in +aTc parasites but focal, unbranched apicoplast morphology in the vast majority (>80%) of -aTc parasites (Figure 7, B and C, and Figure 7- figure supplement 2). Substitution of IPP with FOH or GGOH resulted in a nearly identical apicoplast elongation defect in -aTc parasites. In contrast,

547 substituting IPP with decaprenol resulted in normal apicoplast elongation in both +aTc and -aTc
548 parasites (Figure 7, B and C, and Figure 7- figure supplement 2). The selective ability of
549 decaprenol to rescue apicoplast-branching defects in -aTc conditions strongly supports an essential
550 role for PPS in synthesizing long-chain polyprenyl isoprenoids required for apicoplast biogenesis.

551 To further test this conclusion, we maintained parasites in ±aTc conditions with FOS and
552 IPP for two additional growth cycles (total of five 48-hour cycles, Figure 7A). Parasites cultured
553 +aTc displayed normal elongated apicoplast morphology. In contrast, the -aTc (+FOS and IPP)
554 culture predominantly contained parasites with a dispersed ACP signal indicative of apicoplast
555 loss (Figure 7, D and E, and Figure 7- figure supplement 3). These -aTc parasites also contained a
556 strongly reduced qPCR signal for apicoplast genomic DNA, relative to +aTc parasites (Figure 7F).
557 These results indicate that PPS is essential for apicoplast maintenance and inheritance by daughter
558 parasites such that loss of PPS function (with IPP supplementation) results in parasite progeny
559 lacking the intact organelle. This essential PPS function downstream of IPP synthesis by the MEP
560 pathway is sufficient to explain our observation that blocking pathway activity by FOS or ΔDXS
561 (Figure 1) inhibits apicoplast biogenesis.

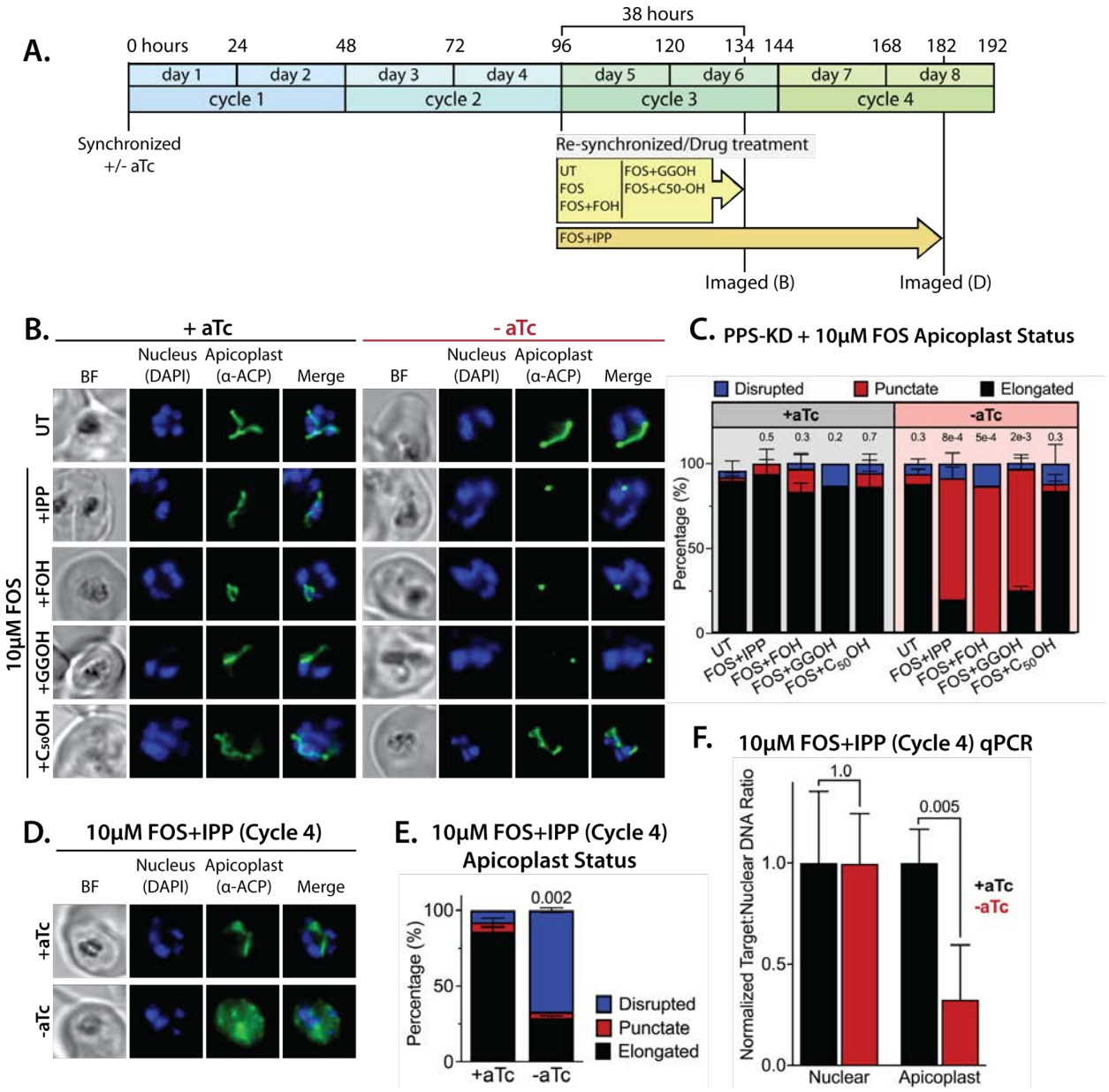


**Figure 7.** PPS is required for apicoplast biogenesis. **(A)** Scheme summarizing growth of synchronized PPS knockdown parasites cultured ±aTc, re-synchronized and treated with 10 μM FOS ±200 μM IPP or 5 μM farnesol (FOH), geranylgeraniol (GGOH), or decaprenol ($C_{50}$-OH) at 96 hours after initial synchronization, and imaged at 134 and 182 hours after initial synchronization. **(B)** Immunofluorescence analysis (IFA) of PPS knockdown parasites cultured as described in panel A and imaged at 134 hours (day 6) after initial synchronization to assess apicoplast morphology ±aTc. **(C)** Statistical analysis of apicoplast morphology for 50 total parasites imaged for each condition in panel A from two independent experiments. Apicoplast morphologies were scored as punctate (focal), elongated, or disrupted (dispersed); counted; and plotted by histogram as the fractional population with the indicated morphology. Error bars represent standard deviations from replicate experiments. Two-tailed unpaired t-test analysis was used to determine the significance of observed population differences compared to untreated (UT)

parasites (P values given above each condition). **(D)** Immunofluorescence analysis of PPS knockdown parasites cultured as described in panel A and imaged at 182 hours (day 8) after initial synchronization to assess apicoplast morphology ±aTc. **(E)** Statistical analysis of apicoplast morphology for 50 total parasites imaged for each condition in panel D and analyzed as in panel C. **(F)** Quantitative PCR analysis of the apicoplast:nuclear (Api:Nu) genome ratio for parasites cultured ±aTc and imaged in panel D, based on amplification of apicoplast TufA (PF3D7_API02900) or nuclear ADSL (PF3D7_0206700) relative to nuclear I5P (PF3D7_0802500) genes. Indicated qPCR ratios were normalized to +aTc in each case and are the average ±SD of two biological replicates. Significance of ±aTc differences was analyzed by two-tailed unpaired t-test to determine the stated P value. All parasite samples collected for IFA were imaged by brightfield (BF) and epifluorescence microscopy, with visualization of parasite nuclei by DAPI staining and apicoplast by an anti-apicoplast ACP antibody.

**Figure supplement 1.** IFA images and analysis of apicoplast morphology in PPS knockdown parasites grown +aTc or -aTc/+IPP (200 μM) for 12 days.

**Figure supplement 2.** Additional IFA images of PPS knockdown parasites treated as in Figure 7B.

**Figure supplement 3.** Additional IFA images of PPS knockdown parasites treated as in Figure 7D.

**No evidence for PPS function in carotenoid synthesis.** Despite its strong sequence similarity to known polyprenyl synthases that catalyze the head-to-tail condensation of isoprenoid precursors, PF3D7_0202700 has also been proposed to catalyze the biochemically distinct head-to-head condensation of 20-carbon GGPP groups into 40-carbon phytoene and thus function as a phytoene synthase (PSY) within a broader pathway of carotenoid biosynthesis proposed to exist in *Plasmodium* parasites (Figure 8A).[53, 59] Polyprenyl synthases and phytoene synthases are mechanistically distinct enzymes that lack significant sequence similarity but are thought to share a common isoprenoid-related protein fold that reflects their ancient divergence from a common ancestral enzyme.[47, 60] Given the mechanistic differences between head-to-tail and head-to-head condensation of isoprenoids (Figure 8A), which involve distinct positioning of substrate pyrophosphate groups within each active site, there is no known enzyme that is capable of catalyzing both reactions.[60] Thus, the proposal of dual PPS and PSY functions for PF3D7_0202700

608 is without biochemical precedent. Nevertheless, we considered whether this protein might also
609 have PSY function and evaluated whether existing observations supported or contradicted a
610 proposed role for this protein in carotenoid biosynthesis.

611 As noted previously, untargeted sequence similarity searches via NCBI BLAST[51] and MPI
612 HHpred[52] with PF3D7_0202700 as the query sequence only identify polyprenyl synthase
613 homologs from bacteria, algae, and plants (Figure 5- figure supplement 3) and fail to identify PSY
614 homologs. Furthermore, targeted pairwise alignments show no evidence of significant sequence
615 homology between PF3D7_0202700 and confirmed eukaryotic or prokaryotic PSY sequences
616 from *Arabidopsis thaliana* (Uniprot P37271, chloroplast-targeted)[61] or *Erwinia herbicola*
617 (*Pantoea agglomerans*, Uniprot D5KXJ0),[62] respectively. Finally, the prior proposal of PSY
618 activity by PF3D7_0202700 was based in part on its sequence similarity to an annotated PSY from
619 *Rubrivivax gelatinosus* bacteria (NCBI accession BAA94032) that also appeared to contain
620 sequence features expected of a head-to-tail polyprenyl synthase.[53] We noted that the functional
621 annotation of this bacterial protein was subsequently revised to a geranylgeranyl-PP synthase
622 (Uniprot I0HUM5),[63] thus explaining its sequence similarity to PF3D7_0202700 and the
623 homology of both proteins to known polyprenyl synthases. On the basis of these sequence
624 analyses, we considered it unlikely that PF3D7_0202700 had dual activity as a PSY.

625 The prior work studied the antiparasitic effects of the squalene synthase inhibitor, zaragozic
626 acid (ZA, also called squalestatin), that inhibited blood-stage *P. falciparum* growth ($EC_{50}$ ~5 μM)
627 and was proposed to specifically target PF3D7_0202700 based on observation of a ~6-fold
628 increase in $EC_{50}$ for parasites episomally expressing a second copy of this protein.[59] We repeated
629 these experiments in Dd2 parasites and observed a similar $EC_{50}$ of ~10 μM for ZA that increased
630 5-fold to ~50 μM in Dd2 parasites episomally expressing PPS-RFP (Figure 8- figure supplement

631 1). However, in contrast to PPS knockdown (Figure 6D), lethal growth inhibition by ZA was not
632 rescued by exogenous IPP (Figure 8- figure supplement 1) and did not affect apicoplast elongation
633 (Figure 8- figure supplement 2). These contrasting phenotypes strongly suggest that PPS, and more
634 broadly the apicoplast, are not uniquely targeted by ZA. The basis for why PPS over-expression
635 reduces parasite sensitivity to ZA is unclear but may reflect drug interactions with broader
636 isoprenoid metabolism outside the apicoplast that are rescued, directly or indirectly, by reaction
637 products of PPS.

638 β-carotene, a 40-carbon carotenoid derived from phytoene, was previously detected by
639 mass spectrometry in extracts of *P. falciparum*-infected erythrocytes and suggested to be
640 biosynthesized by parasites based on the lack of detection in extracts of uninfected erythrocytes.[53]
641 Using our PPS knockdown line, we tested whether translational repression of PF3D7_0202700
642 impacted detectable levels of β-carotene in parasites, as predicted to occur if PPS also functioned
643 as a PSY. After synchronization, PPS knockdown parasites were grown ±aTc for 120 hours and
644 harvested at the end of the third intraerythrocytic growth cycle, which immediately precedes the
645 growth defect observed in Figure 6D. Saponin pellets of these parasites were extracted in acetone
646 and analyzed by liquid chromatography/tandem mass spectrometry for β-carotene (Figure 8- figure
647 supplement 3). We observed indistinguishable low levels of β-carotene in both samples (Figure
648 8B), providing no evidence that PPS plays a role in carotenoid biosynthesis.

649 Although uninfected erythrocytes washed in AlbuMAX-free RPMI lacked detectable β-
650 carotene, we observed that extracts of uninfected erythrocytes incubated in complete RPMI
651 medium containing AlbuMAX I had β-carotene levels that were nearly identical to extracts of
652 parasite-infected erythrocytes (Figure 8B). Analysis of AlbuMAX (ThermoFisher catalog
653 #11020021) by mass spectrometry revealed modest levels of β-carotene (Figure 8- figure

supplement 4), consistent with the bovine origin of AlbuMAX (lipid-rich bovine serum albumin) and the plant-based diet of these animals expected to contain β-carotene. These results are sufficient to explain the presence of carotenoids like β-carotene in parasite extracts. In summary, we find no evidence that PPS function contributes to β-carotene levels in *P. falciparum*-infected erythrocytes, which we suggest non-specifically take up exogenous plant-derived β-carotene associated with AlbuMAX in the culture medium.

Parasite-infected erythrocytes were previously reported to incorporate $^{3}$H-labeled GGPP into biosynthetic products that had reverse-phase HPLC retention times similar to all-trans-lutein or β-carotene standards, suggesting de novo synthesis of these isoprenoid products.[53] Because the extracted products were radioactive, their identity could not be directly confirmed by tandem mass spectrometry. To directly test if blood-stage *P. falciparum* parasites incorporate isoprenoid precursors into β-carotene, as predicted for active biosynthesis, we cultured the PfMev parasites in 50 μM of 2-$^{13}$C-mevalonate in the presence of 10 μM FOS. This strategy was chosen to inhibit MEP pathway activity, ensure full $^{13}$C-labeling of the endogenous IPP and DMAPP precursor pool produced by the cytoplasmic bypass enzymes, and result in a distinguishable 8 Da mass increase for any β-carotene derived from de novo synthesis. We previously showed that this strategy results in complete $^{13}$C-labeling of endogenous IPP and FPP.[29] Parasites were expanded to high parasitemia over several days under $^{13}$C-labeling conditions before extraction and analysis by mass spectrometry. Although we readily detected unlabeled β-carotene (m/z 536.4), which we attribute to culture medium AlbuMAX, we were unable to detect $^{13}$C-labeled β-carotene (m/z 544.4) (Figure 8C). In contrast to the parasite analysis, we readily detected fully $^{13}$C-labeled β-carotene (m/z 576.6) produced by *E. coli* bacteria engineered to biosynthesize β-carotene[64] and grown in minimal M9 medium with uniformly labeled $^{13}$C-glucose as the sole carbon source (Figure 8D). In

677 summary, we find no evidence for PSY function by PF3D7_0202700 or for de novo carotenoid
678 synthesis by blood-stage *P. falciparum* parasites. Collectively, our data strongly support the
679 conclusion that PF3D7_0202700 functions exclusively as a polyprenyl synthase required for
680 apicoplast biogenesis.

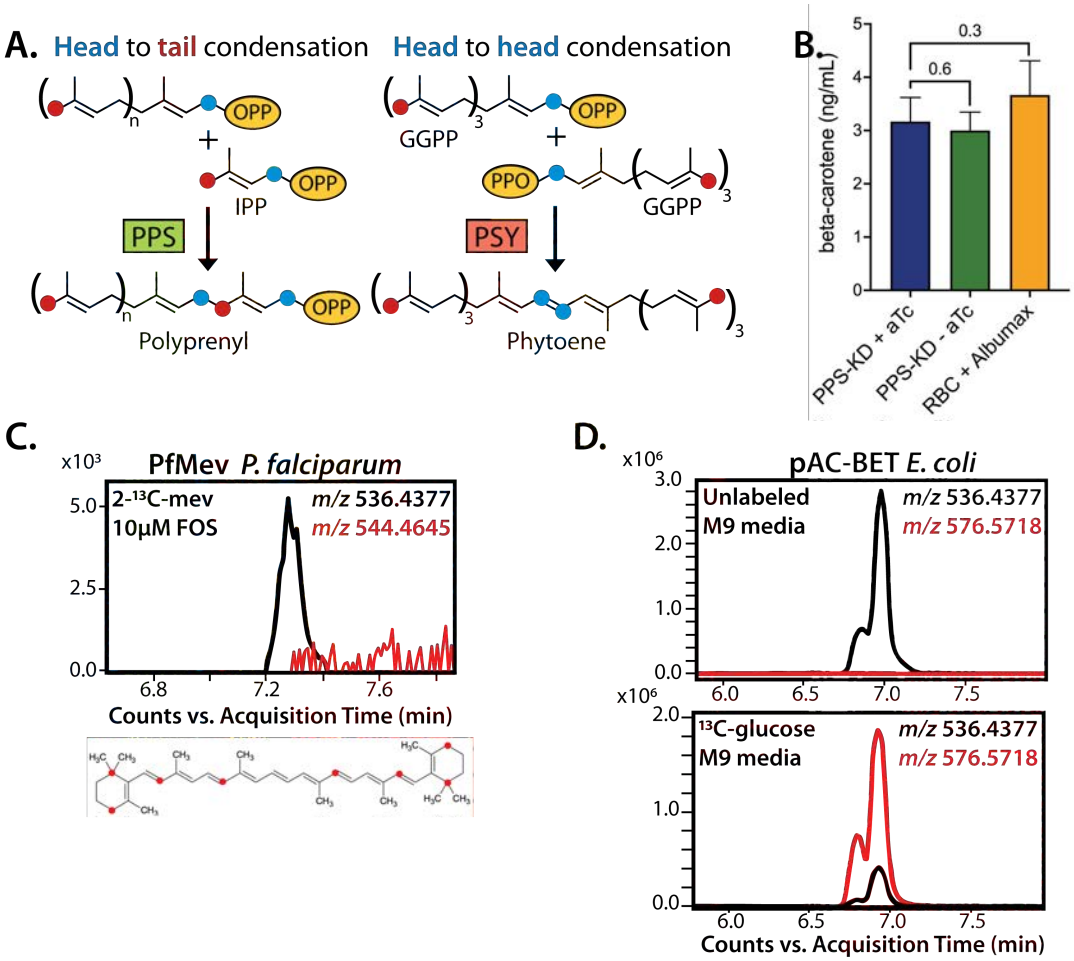


681
682
683 **Figure 8.** No evidence that PPS contributes to carotenoid synthesis by *P. falciparum*. **(A)**
684 Schematic depiction of head-to-tail arrangement of prenyl groups during polyprenyl-PP synthesis
685 versus head-to-head arrangement of geranylgeranyl-PP groups during phytoene synthesis. **(B)**
686 Mass spectrometry determination of unlabeled β-carotene levels in PPS knockdown parasites
687 grown for 6 days ±aTc or in uninfected red blood cells incubated in complete media containing
688 Albumax. Measured β-carotene levels are the average ±SD of 3 biological replicates, whose
689 differences were analyzed by two-tailed unpaired t-test for significance (P values given relative to
690 +aTc sample). **(C)** Intensity versus retention time plot for liquid chromatography-mass
691 spectrometry determination of unlabeled and $^{13}$C-labeled β-carotene in NF54 PfMev parasites
692 cultured for 6 days in 50 µM 2-$^{13}$C-mevalonate and 10 µM fosmidomycin. Below: schematic
693 depiction of the 8 carbon atoms in β-carotene expected to be labeled with $^{13}$C for synthesis from

IPP derived from 2-$^{13}$C-mevalonate in PfMev parasites. **(D)** Intensity versus retention time plot for liquid chromatography-mass spectrometry determination of unlabeled and $^{13}$C-labeled β-carotene in pAC-BETAipi *E. coli* grown in unlabeled or fully $^{13}$C-labeled glucose as the sole carbon source in M9 minimal media. The two peaks reflect the presence of an isomeric mix of all-trans and cis β-carotene produced by the pAC-BETAipi *E. coli*, as previously reported.[64]

**Figure supplement 1.** 48-hour growth inhibition curves for treatment of Dd2 parasites with zaragozic acid without or with episomal expression of PPS-RFP or 200 μM IPP.

**Figure supplement 2.** Epifluorescence microscopy images of D10 parasites treated with 160 μM zaragozic acid as synchronized rings and imaged for $ACP_L$-GFP and Hoescht 36 hours later as multinuclear schizonts.

**Figure supplement 3.** Fragment ion spectrum for unlabeled beta-carotene determined by tandem mass spectrometry of β-carotene commercial standard.

**Figure supplement 4.** Intensity versus retention time plot for liquid chromatography-mass spectrometry determination of unlabeled β-carotene in Albumax I.

## DISCUSSION

Biosynthesis of the isoprenoid precursors, IPP and DMAPP, is a well-established essential function of the *Plasmodium* apicoplast, but prior work has focused nearly exclusively on the critical roles of isoprenoids for diverse cellular processes outside this organelle.[7, 11, 15, 20] We have elucidated a novel arm of isoprenoid metabolism within the apicoplast that is required for biogenesis of this critical organelle (Figure 9). This discovery expands the paradigm for isoprenoid utilization by malaria parasites, uncovers a novel essential feature of apicoplast biology, and identifies a key enzyme in this pathway suitable for development as a therapeutic target.

**Implications for general understanding of apicoplast functions.** Our study, which was inspired by prior hints in the literature,[25-27] firmly establishes a novel essential role for MEP pathway activity in supporting apicoplast biogenesis, in addition to its recognized role producing IPP required outside this organelle. The dual roles of this pathway in both apicoplast-specific and broader parasite cellular biology provide a clear exception to the prevailing binary model of blood-

stage apicoplast metabolism that pathway functions in this organelle can be cleanly segregated into those required for organelle maintenance versus those producing an essential anabolic output.[11, 13, 15, 65] Thus, IPP synthesis by the MEP pathway requires apicoplast maintenance, which in turn depends on IPP synthesis. The two processes are convoluted and interdependent.

Our results also support the emerging paradigm[12, 16-18] that inhibition of apicoplast maintenance pathways can kill parasites with first-cycle kinetics that defy the delayed-death phenotype commonly observed for translation-blocking antibiotics such as doxycycline that target organelle housekeeping.[6, 12] Indeed, blocking IPP synthesis causes same-cycle defects in apicoplast biogenesis, which are expected to produce non-viable parasite progeny independent of lethal dysfunctions in isoprenoid-dependent metabolism outside the organelle. Analysis of the timing of FOS-induced defects in apicoplast branching also provides an unexpected and incisive window into the differential compartmentalization of IPP essentiality in parasites. We observed that FOS-treated parasites display apicoplast-elongation defects in early schizogony but continue to divide nuclear DNA and transition into mature schizonts before stalling prior to segmentation (Figure 1A). Thus, the critical role of IPP for apicoplast biogenesis precedes the broader cellular need for IPP outside the organelle in mature schizonts, suggested by recent works to predominantly reflect essential roles for IPP-dependent protein prenylation.[15, 30] Although MEP pathway activity begins in ring-stage parasites,[31, 32] we observed identical inhibition of apicoplast elongation in schizonts independent of whether FOS was added to rings concomitant with synchronization or to trophozoites 12 hours after synchronization (Figure 1A). This observation suggests that IPP utilization in the apicoplast depends on de novo synthesis rather than a pre-existing metabolite pool, possibly because IPP does not accumulate in the apicoplast and/or that IPP synthesis within the organelle is differentially partitioned for export and internal utilization.

**Why does apicoplast biogenesis depend on IPP synthesis?** The essential function of PPS in apicoplast maintenance is sufficient to explain the apicoplast reliance on IPP synthesis unveiled by FOS treatment of parasites. Although the dominant polyprenyl-PP product of apicoplast PPS in parasites remains uncertain, sequence features, prior in vitro enzymology, and the ability of exogenous decaprenol but not GGOH or FOH to rescue PPS knockdown indicate that linear polyprenyl-PP products longer than 4 and as long as 10 isoprene units are critical for apicoplast maintenance .[24] Prior work suggested a dual function for PF3D7_0202700 as a phytoene synthase (PSY) that also condenses isoprenoid precursors,[53, 59] but we found no evidence to support this proposed PSY function or carotenoid biosynthesis more broadly. Synthesis of octaprenyl-PP by PF3D7_0202700 was previously proposed to be critical for ubiquinone biosynthesis in the parasite mitochondrion.[24] Localization of this protein to the apicoplast (Figure 5) and observation that exogenous IPP rescues the grown defects of its knockdown (Figure 6D) strongly suggest that its activity is not required for mitochondrial ubiquinone biosynthesis and that its essential function is specific to the apicoplast.

Plant chloroplasts synthesize linear polyprenyl isoprenoids to serve a wide variety of functions that are only partially understood but include key roles in light harvesting and photosynthesis, oxidative stress protection, and as precursors of signaling and defense molecules that function outside the chloroplast (e.g., abscisic acid, gibberellins, and terpenes).[66-68] The *Plasmodium* apicoplast has lost photosynthesis capabilities and has uncertain carotenoid and terpene synthesis capacity. Volatile terpenes[69] and carotenoids[53] have been detected in *P. falciparum*-infected erythrocytes, but the parasite genome lacks enzyme homologs of the relevant synthases required for terpene and carotenoid biosynthesis. [1, 7] Furthermore, we found no evidence

of de novo β-carotene synthesis by parasites, and results herein as well as recent studies[70, 71] indicate that these metabolites can derive from erythrocyte and/or culture medium sources rather than parasite-specific synthesis. Thus, these known functions in chloroplasts seem uncertain or unlikely to explain apicoplast reliance on longer-chain polyprenyl synthase activity in malaria parasites. Longer-chain polyprenyl-PPs and related dolichols serve as membrane-bound glycan carriers for protein glycosylation, but these activities in *Plasmodium* appear to occur in the endoplasmic reticulum as they do in other organisms.[20, 72, 73]

Linear polyprenyl alcohols have been found to be important components of plant membranes, especially chloroplast membranes, where they are proposed to modulate membrane structure, fluidity, and dynamics.[66, 68, 74, 75] In the absence of other known roles for longer-chain polyprenyl-PPs in the apicoplast, we hypothesize that linear polyprenols or polyprenyl phosphates may serve as critical components of the apicoplast membranes and be required for maintaining membrane fluidity during organelle biogenesis (Figure 9). A prior mass spectrometry-based lipidomics study of isolated apicoplasts focused primarily on the fatty acid and phospholipid composition of this organelle and did not characterize isoprenoid components.[76] Selective isotopic labeling of parasite-synthesized isoprenoids by 2-$^{13}$C-mevalonate in the PfMev line, combined with apicoplast isolation and our PPS knockdown line, can potentially identify specific apicoplast isoprenoids whose synthesis depends on PPS activity and thus clarify why apicoplast biogenesis requires longer-chain polyprenyl synthase activity.

Independent of its specific role in apicoplast biogenesis, PPS function is critical for parasite survival and thus constitutes a new essential arm of isoprenoid metabolism in the apicoplast suitable for development as a therapeutic target. BLAST analysis of the human genome using the PPS protein sequence as query reveals a variety of polyprenyl synthase homologs with modest 20-

30% sequence identity to 25-50% of the PPS sequence. The substantial sequence differences with human orthologs will facilitate selective targeting of PPS by chemical inhibitors. Identification of PPS as an apicoplast-targeted enzyme indicates that new metabolic pathways and functions remain to be discovered and/or localized to the apicoplast. These novel functions, which are predicted to be required for organelle maintenance, will enhance our understanding of fundamental apicoplast biology and provide new candidate drug targets for antimalarial therapies.

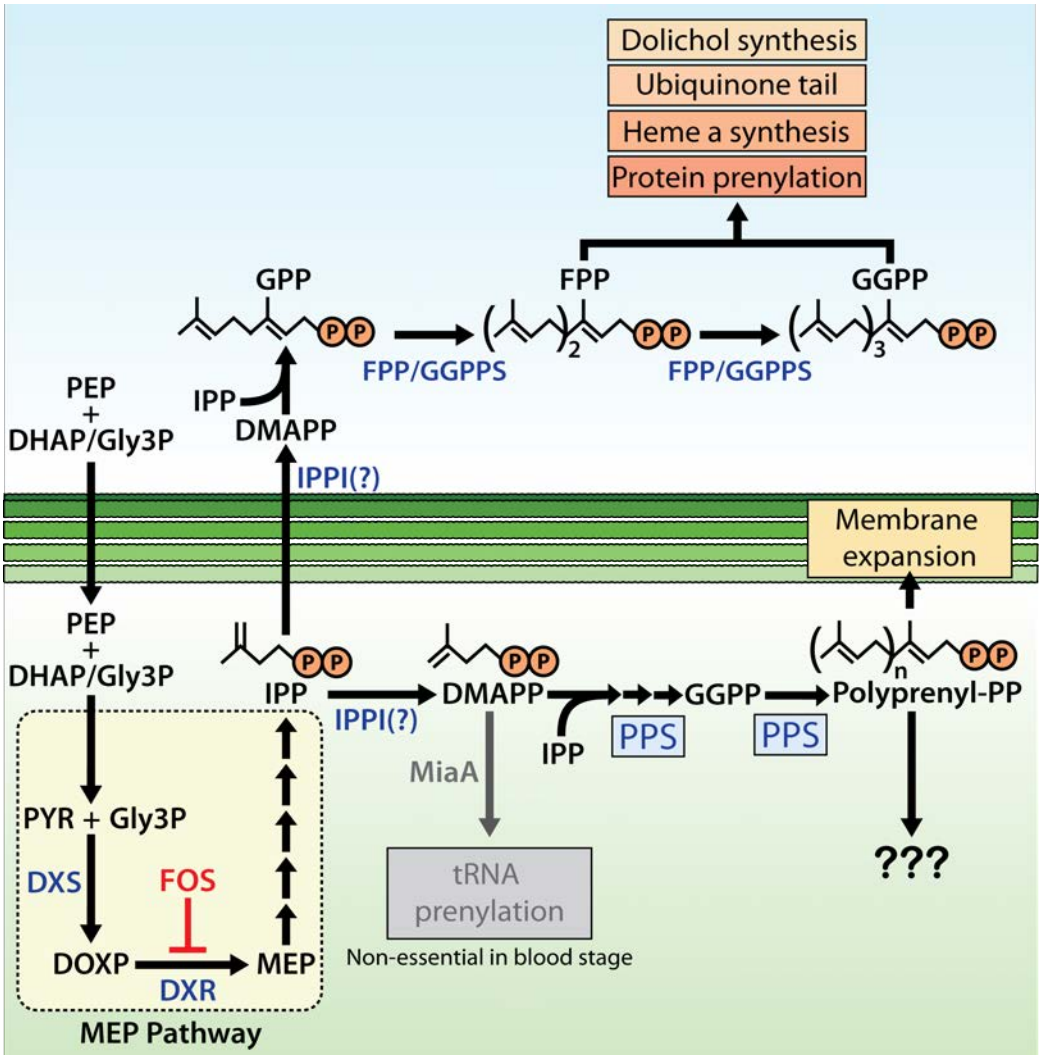


**Figure 9**. Schematic diagram of apicoplast isoprenoid metabolism in blood-stage *P. falciparum* parasites. PK = pyruvate kinase II, TPI = triose phosphate isomerase, IPPI = IPP isomerase, PEP = phosphoenolpyruvate, DHAP = dihydroxyacetone phosphate, PYR = pyruvate, Gly3P = glyceraldehyde-3-phosphate. Question marks indicate uncertainty in the identity of the proposed IPP isomerase and in the role of polyprenyl isoprenoid products of PPS in apicoplast biogenesis.

## MATERIALS AND METHODS

**Materials**: All reagents were of the highest purity commercially available. The vendor and catalog number are given for individual compounds when first mentioned.

**Fluorescence Microscopy:** For live-cell experiments, parasite samples were collected at 38 hours after synchronization with 5% D-sorbitol (Sigma S7900). Parasite nuclei were visualized by incubating samples with 1-2 μg/ml Hoechst 33342 (Thermo Scientific Pierce 62249) for 10-20 minutes at room temperature. The parasite apicoplast was visualized in D10[28] or NF54 mevalonate-bypass[29] cells using the $ACP_L$-GFP expressed by both lines. The parasite mitochondrion was visualized by incubating parasites with 10 nM MitoTracker Red CMXROS (Invitrogen Life Technologies M7512) for 15 minutes prior to wash-out and imaging. For immunofluorescence assay (IFA) experiments, parasites were fixed, stained, and mounted as previously described.[77] For IFA images, the parasite apicoplast was visualized using a polyclonal rabbit anti-ACP antibody[78] and an anti-rabbit fluorescent 2˚ antibody, the nucleus was stained with ProLong Gold Antifade Mountant with DAPI (Invitrogen Life Technologies P36931), and PPS-GFP was visualized with a Goat anti-GFP antibody (Abcam ab5450). Images were taken on DIC/brightfield, DAPI, GFP, and RFP channels using either a Zeiss Axio Imager or an EVOS M5000 imaging system. Fiji/ImageJ was used to process and analyze images. All image adjustments, including contrast and brightness, were made on a linear scale.

For phenotypic analyses, apicoplast morphologies for each experimental condition were assessed for 25 parasites in each of two biological replicate experiments (50 parasites total per condition). Apicoplast morphologies were scored as elongated, focal, or dispersed; counted; and plotted by histogram as the fractional population with the indicated morphology. Statistical

significance of observed differences from untreated parasites was assessed in GraphPad Prism 9 by two-tailed unpaired t test. P values were rounded to one significant figure, and non-significance was concluded for differences with P values >0.05.

**Inhibition and Rescue of Apicoplast Biogenesis:** $ACP_L$-GFP D10 and NF54 PfMev parasites were synchronized with 5% (w/v) D-sorbitol for 10 minutes at room temperature and returned to culture in 10 μM fosmidomycin (Invitrogen Life Technologies F23103), 100 nM atovaquone (Caymen Chemicals 23802), 2 μM DSM1,[79] 6 μM blasticidin-S (Invitrogen Life Technologies R21001), 5 nM WR99210 (Jacobus Pharmaceuticals), 160 μM zaragozic acid/squalestatin (Caymen Chemicals 17452), or 2 μM MMV019313 (ChemDiv C498-0579). For FOS experiments, parasites were left in FOS only or supplemented with 5 μM farnesol (Sigma F203), 5 μM geranylgeraniol (Sigma G3278), 5 μM decaprenol (Isoprenoids polyprenol C50), 5 μM β-carotene (Sigma C9750), 50 μM DL-mevalonolactone (Cayman Chemicals 20348), or 200 μM IPP ($NH_4^+$ salt, Isoprenoids IPP001). All parasites were cultured for 36 hours after synchronization and then imaged by live-cell fluorescence microscopy to monitor apicoplast status. All concentrations reflect the final concentration in culture medium.

**Parasite synchronization:** Parasites were synchronized to the ring stage either by treatment with 5% D-sorbitol (Sigma S7900) or by first magnet-purifying schizonts and then incubating them with uninfected erythrocytes for 5 hr followed by treatment with sorbitol. Results from growth assays and microscopy analyses using either of these synchronization methods were indistinguishable within error, and 5% sorbitol was used unless stated otherwise.

852 **Delayed Mevalonate-Rescue Assay:** NF54 PfMev parasites were synchronized with 5% (w/v)
853 D-sorbitol for 10 minutes at room temperature and returned to culture in 10 μM fosmidomycin. 50
854 μM DL-mevalonate was added to cultures immediately or after 30, 34, or 38 hours post
855 synchronization. Parasitemia was measured by flow cytometry every 24 hours. After 60 hours
856 post-synchronization, parasites from each mevalonate time point were cloned out by limiting
857 dilution. Apicoplast status of all isolated clones was evaluated by live-cell $ACP_L$-GFP
858 fluorescence. $ACP_L$-GFP signal was observed for the presence of distinct branching morphology
859 (apicoplast intact) or the presence of scattered punctate signals throughout the cytosol (apicoplast
860 disruption). A total of 9, 17, 18, and 5 clones from the 0, 30, 34, and 38-hour rescue time-points,
861 respectively, were evaluated by microscopy (only 5 clones returned from the 38-hour rescue time
862 point). Apicoplast (SufB: Pf3D7_API04700) and nuclear (PPS: Pf3D7_0202700) genome PCR
863 (primers 4/5 and 1/2) and mevalonate-dependence growth assays were done on 2 clones from each
864 time point to confirm apicoplast status.
865
866 **Parasite Culturing and Transfection:** All experiments were performed using *Plasmodium*
867 *falciparum* Dd2, $ACP_L$-GFP D10[28], or $ACP_L$-GFP NF54 PfMev[29] parasite strains. Parasite
868 culturing was performed in Roswell Park Memorial Institute medium (RPMI-1640, Thermo Fisher
869 23400021) supplemented with 2.5 g/L Albumax I Lipid-Rich BSA (Thermo Fisher 11020039), 15
870 mg/L hypoxanthine (Sigma H9636), 110 mg/L sodium pyruvate (Sigma P5280), 1.19 g/L HEPES
871 (Sigma H4034), 2.52 g/L sodium bicarbonate (Sigma S5761), 2 g/L glucose (Sigma G7021), and
872 10 mg/L gentamicin (Invitrogen Life Technologies 15750060). Cultures were generally
873 maintained at 2% hematocrit in human erythrocytes obtained from the University of Utah Hospital
874 blood bank, at 37 ˚C, and at 5% $O_2$, 5% $CO_2$, 90% $N_2$. Parasite-infected erythrocytes were

875 transfected in 1X cytomix containing 50-100 µg midi-prep DNA by electroporation in 0.2 cm
876 cuvettes using a Bio-Rad Gene Pulser Xcell system (0.31 kV, 925 µF). Transgenic parasites were
877 selected on the basis of plasmid resistance cassettes encoding human DHFR[36], yeast DHOD[79], or
878 blasticidin-S deaminase (BSD)[35] and cultured in 5 nM WR99210, 2 µM DSM1, or 6 µM
879 blasticidin-S, respectively. Gene-edited Dd2 parasites that contained PPS (PF3D7_0202700)
880 tagged with the aptamer/TetR-DOZI cassette[57] were maintained in 0.5-1 µM anhydrotetracycline
881 (Caymen Chemicals 10009542). Genetically modified parasites were genotyped by PCR and/or
882 Southern blot, as previously described.[80] For western blot and IFA studies of PPS-GFP in
883 apicoplast-disrupted Dd2 parasites, transgenic parasites were cultured >7 days in 5 nM WR99210,
884 1 µM doxycycline (Sigma D9891), and 200 µM IPP to induce stable apicoplast loss prior to
885 parasite harvest.
886
887 **Parasite Growth Assays:** Parasite growth was monitored by diluting asynchronous or sorbitol-
888 synchronized parasites to ~0.5% parasitemia and allowing culture expansion over several days
889 with daily media changes. Parasitemia was monitored daily by flow cytometry by diluting 10 µl
890 of each parasite culture well from each of two to three biological replicate samples into 200 µl of
891 1.0 µg/ml acridine orange (Invitrogen Life Technologies A3568) in phosphate buffered saline
892 (PBS) and analysis on a BD FACSCelesta system monitoring SSC-A, FSC-A, PE-A, FITC-A, and
893 PerCP-Cy5-5-A channels. Daily parasitemia measurements for asynchronous cultures were plotted
894 as function of time and fit to an exponential growth equation using GraphPad Prism 9.0. For $EC_{50}$
895 determinations, synchronous ring-stage parasites were diluted to 1% parasitemia and incubated
896 with variable drug concentrations for 48-72 hours without media changes. Parasitemia was
897 determined by flow cytometry in biological duplicate samples for each drug concentration,

898 normalized to the parasitemia in the absence of drug, plotted as a function of the log of the drug
899 concentration (in nM or μM), and fit to a 4-parameter dose-response model using GraphPad Prism
900 9.0.
901
902 **Cloning and Episomal Expression of PPS:** The gene encoding PPS (PF3D7_0202700) lacks
903 introns and was cloned by PCR from Dd2 parasite genomic DNA using primers designed for
904 insertion into the XhoI/AvrII sites of pTYEOE (yeast DHOD positive selection cassette)[81] and
905 pTEOE (human DHFR positive selection cassette)[55] vectors in frame with C-terminal RFP and
906 GFP tags, respectively. These vectors are designed to drive episomal protein expression using the
907 HSP86 promoter and for co-transfection with plasmid pHTH that contains the piggyBac
908 transposase[82] for integration into the parasite genome. A single forward primer was used for PPS
909 cloning into both vectors (primer 1) while reverse primers were vector-specific (primers 2 and 3)
910 Cloning was completed using ligation-independent cloning (QuantaBio RepliQa HiFi Assembly
911 Mix). Cloning products were transformed into Top10 chemically competent cells, and bacterial
912 clones were selected for carbenicillin (Sigma C3416) resistance. Correct plasmid sequence in
913 isolated clonal bacteria was confirmed by both AscI/AatII (NEB) restriction digest and Sanger
914 sequencing (University of Utah DNA Sequencing Core). 100 μg of either purified PPS-RFP-
915 TyEOE or PPS-GFP-TEOE in combination with 25 μg of the pHTH transposase plasmid was
916 transfected into Dd2 parasites by electroporation, as described above. Transfected parasites were
917 allowed to expand in the absence of drug for 48 hours before selection with either 2 μM DSM1 or
918 5 nM WR99210 for PPS-RFP-TyEOE or PPS-GFP-TEOE respectively. Stable, drug-resistant
919 parasites returned from transfection in 3-6 weeks.
920

**PPS Gene-Editing to Enable Ligand-Dependent Regulation of Protein Expression:** Crispr/Cas9-stimulated repair by double-crossover homologous recombination was used to tag the PPS gene (PF3D7_0202700) to encode a C-terminal hemagglutinin (HA)-FLAG epitope tag and the 3' 10X aptamer/TetR-DOZI system[57] to enable regulated PPS expression using anhydrotetracycline. Guide RNA sequences corresponding to TGATATAAAACAAAGTAGCG, CGTGCTAGTTCTATTTTTGC, and GATGATTCAAATAAAAGAAG (primers 6-11) were cloned into a modified version of the previously published pAIO vector,[83] in which the BtgZI site was replaced with a unique HindIII site to facilitate cloning (primers 12 and 13). To tag the PPS gene, a donor pMG75[57] repair plasmid was prepared by PCR-amplifying 635 bp of the 3' coding sequence and 679 bp of the 3' untranslated region (UTR) as homology flanks to the PPS gene, fusing these fragments together by PCR with an AflII site in between (679 bp 3' UTR-AflII-635 bp 3' coding sequence), and inserting this fused fragment into the AscI and AatII sites of the pMG75 vector (primers 14-17). A shield mutation was introduced to the 3' end of the coding-sequence homology flank corresponding to the gRNA sequence TGATATAAAACAAAGTAGCG. This mutation (introduced using primer 18) ablated the CRISPR PAM sequence AGG that immediately following the gRNA sequence above by mutating it to AAG, resulting in a silent mutation of the Glu523 codon from GAG to GAA. Sanger sequencing confirmed the correct sequence of the homology flanks inserted into the pMG75 vector. PCR analysis of the final pMG75 vector using primers 39-40 revealed that only 9 copies of the aptamer sequence were retained. Before transfection, the pMG74 vector was linearized by AflII digestion performed overnight at 37˚ C, followed by deactivation with Antarctic Phosphatase (NEB M0289S).

Dd2 parasites were transfected with 50 µg of pAIO Cas9/gRNA vector and 50 µg of the linearized pMG75 donor plasmid, as described above. Parasites were selected on the basis of the BSD resistance cassette encoded by the pMG75 plasmid and returned from transfection after 4-6 weeks. Gene-edited Dd2 parasites resulting from transfection with pAIO Cas9/gRNA-4 (produced with primers 10/11) contained PPS (PF3D7_0202700) tagged with the aptamer/TetR-DOZI cassette[57] and were maintained in 0.5-1 µM anhydrotetracycline (Caymen Chemicals 10009542). Genetically modified parasites were genotyped by Southern blot, as previously described.[80] Briefly, genomic DNA from the polyclonal parasites that returned from transfection was digested with BamHI and SpeI (New England Biolabs) and transferred to membrane (Nytran SuPerCharge) using the TurboBlotter system (VWR 89026-838). A DNA probe consisting of the 5' 750 bp of the PPS gene was produced by PCR (primers 16/17). Probe labeling, hybridization, and visualization was performed using the AlkPhos Direct Labeling and Detection System (VWR 95038-288) and CDP-Star reagent (VWR 95038-292). The Southern blot confirmed complete integration into the PPS locus without evidence for unmodified parasites, and the polyclonal parasites were used for all subsequent experiments.

**Analysis of PPS transcript levels:** Cultures of PPS-aptamer/TetR-DOZI parasites were synchronized in 5% D-sorbitol and grown for 72 or 120 hours ±aTc prior to harvest. 4-ml cultures at approximately 10% were harvested by centrifugation (2000 rpm for 3 min.) and stored at -20 ˚C until use. Total RNA was isolated from frozen parasite-infected blood pellets using a modified Trizol (Invitrogen) extraction protocol. 5 mL Trizol (Invitrogen) was added to thawed pellets on ice, pipetted 20-30 times to resuspend, and pulse-vortexed 20 times for 15 s. 2 mL chloroform was added to each sample and vortexed, incubated on ice for 5 minutes, then spun for 10 minutes at 4C

966 at 5000rpm without brake. The top, aqueous layer (approximately 3 mL) was transferred to a new
967 tube. 5 mL of isopropanol was added to each sample, gently mixed, and incubated at -80 ˚C for 20
968 minutes or -20 ˚C overnight. Samples were spun at 5000 rpm for 30 min, washed with freshly-
969 made solution of 70% ethanol, then spun again for 10 min. Ethanol was removed and pellets were
970 dried 30 min on ice. RNA pellets were resuspended in RNAse-free water, quantitated, and used
971 immediately or stored at -80 ˚C. 1 µg of RNA was DNAse-treated and reverse-transcribed using
972 Superscript IV kit (Invitrogen) with the addition of gene-specific reverse primers 31-38.
973 Subsequent cDNA was analyzed in duplicate through qPCR reactions with SYBR Green
974 fluorescent probe (Invitrogen) in a Roche Lightcycler. Cp values for PPS (primers 35-36) were
975 normalized to the average of 2 nuclear-encoded control genes (I5P, PF3D7_0802500; ADSL,
976 PF3D7_0206700; primers 31-34), then used to calculate relative +aTC/-aTC RNA abundance for
977 each of two biological replicates. Significance of the observed difference was evaluated by two-
978 tailed unpaired t-test using GraphPad Prism 9.0.
979
980 **Synchronous Growth Assays of PPS Knockdown Parasites:** Dd2 parasites tagged at the
981 genomic PPS locus with the aptamer/TetR-DOZI system were synchronized by 5% D-sorbitol to
982 ring-stage parasites and allowed to expand ±aTc in two or three biological replicate samples.
983 Parasitemia values were measured daily by flow cytometry and plotted as the average ±SD of
984 replicate samples. For growth-rescue experiments, synchronous parasites were allowed to expand
985 ±aTc, and -aTc plus 200 µM IPP, 5 µM farnesol (FOH), 5 µM geranylgeraniol (GGOH), or 5 µM
986 decaprenol ($C_{50}$-OH). For growth-rescue experiments involving fosmidomycin (FOS), PPS KD
987 parasites were synchronized to rings with 5% D-sorbitol and grown for 4 days (96 hours) ±aTc.
988 After 96 hours, all culture wells were synchronized again with 5% D-sorbitol and supplemented

with 10 μM FOS and 200 μM IPP, 5 μM FOH, 5 μM GGOH, or 5 μM decaprenol. Parasites were cultured for another 38 hours before harvest at 134 total hours post-initial synchronization for IFA analysis of apicoplast morphology. Parasites grown ±aTc with 10 μM FOS and 200 μM IPP were allowed to expand for an additional 48 hours and harvested at 182 hours post-initial synchronization for analysis by IFA and qPCR for apicoplast morphology and apicoplast:nuclear genome levels, respectively.

**qPCR Analysis of Apicoplast:Nuclear genomic DNA levels:** Genomic DNA was extracted from parasite samples grown ±aTc with 10 μM FOS and 200 μM IPP and harvested at 182 hours post-initial synchronization. DNA extraction was performed using the QIAmp DNA Blood Mini Kit (Qiagen 51104). Primers for qPCR were designed to amplify a 120-140 bp region of an apicoplast gene (TufA, PF3D7_API02900, primers 35-36) and each of two nuclear genes (I5P, PF3D7_0802500; ADSL, PF3D7_0206700; primers 31-34). Approximately 100 ng of DNA was amplified in each of two biological replicates with PowerUp SYBR Green Master Mix (ThermoFisher A25741) in a 96-well plate with 20 μl reaction volume on a Quantstudio3 Real Time PCR system. Specificity of primer amplification was confirmed for every sample by identifying only one melting temperature for the product of each qPCR reaction. Abundance of apicoplast relative to nuclear DNA was determined by comparative $C_t$ analysis,[84] with amplification of TufA (apicoplast) and I5P (nuclear) and calculation of $2^{\Delta Ct}$, where $\Delta Ct = Ct_{TufA} - Ct_{I5P}$. As a positive control, abundance of a second nuclear gene (ADSL) relative to I5P was calculated similarly. The $2^{\Delta Ct}$ value for TufA or ADSL was normalized to +aTc for each gene to determine a normalized target gene:control gene DNA abundance. Error bars represent the

standard deviation between replicates, and P values were determined by two-tailed unpaired t-test in GraphPad Prism 9.0.

**MiaA Gene Disruption:** The gene encoding MiaA (PF3D7_1207600) was disrupted in the NF54 PfMev line using CRISPR/Cas9 and gene deletion by double-crossover homologous recombination, similar to the recently described disruption of the DXPR gene (PF3D7_1467300).[29] Homology arm regions (411 bp for the 5' arm and 540 bp for the 3' arm) were PCR-amplified from genomic DNA with primers 19-22 and cloned into the vector pRS[29] using ligation-independent cloning (In-Fusion, Clontech). A guide RNA with sequence AATAACGATATTAAATGTAA was cloned into a modified pAIO vector called pCasG[85] using primers 23 and 24. 75 µg of pRS-miaA-KO plasmid was combined with 75 µg of the pCasG guide RNA plasmid and transfected into NF54 PfMev parasites. Transfected parasites were allowed to expand for 48 hours in 50 µM mevalonate before selection with 5 nM WR99210 and 50 µM mevalonate. Parasites returning from positive selection were genotyped by PCR using primers 25-30. Asynchronous growth of ΔMiaA PfMev parasites ±Mev compared to parental PfMev parasites was performed on biological duplicate samples. Average parasitemia values ±SD were plotted versus time and fit to an exponential growth equation in GraphPad Prism 9.0. Apicoplast (SufB: Pf3D7_API04700) and nuclear (LDH: PF3D7_1324900) genome PCR was performed to confirm apicoplast status in parental PfMev and ΔMiaA parasites, as previously reported.[29]

**Western Blots:** Samples of episomal PPS-GFP Dd2 or endogenously HA-FLAG-tagged PPS Dd2 parasites were harvested by centrifugation and treated with 0.05% saponin (Sigma 84510) in PBS for 5 min at room temperature and spun down by centrifuge at 5,000 rpm for 30 minutes at 4°C.

2% SDS was added to saponin pellets and resuspended by sonication. Parasites were incubated in 2% SDS overnight at 4°C. 5x Sample buffer containing beta-mercaptoethanol (BME) was added to parasite samples before heating at 95°C for 5 minutes and centrifuging at 13,000 rpm for 5 minutes. Samples were fractionated by SDS-polyacrylamide gel electrophoresis (PAGE) using 10% acrylamide gels run at 120 V in the BIO-RAD mini-PROTEAN electrophoresis system. Fractionated proteins were transferred from polyacrylamide gel to a nitrocellulose membrane at 100V for one hour using the BIO-RAD wet transfer system. Membranes were blocked in 1% casein/PBS for one hour at room temperature and then probed with primary antibody overnight at 4°C and secondary antibody at room temperature for 1 hour. Episomal PPS-RFP parasite samples were probed with 1:1000 mouse anti-RFP (Invitrogen Life Technologies MA5-15257) and 1:10,000 donkey anti-mouse DyLight800 (Invitrogen Life Technologies SA5-10172). Endogenous HA-FLAG-tagged PPS parasite samples were probed with Roche rat anti-HA monoclonal 3F10 primary (Sigma 11867423001) and donkey-anti-rat DyLight800 (Invitrogen Life Technologies SA5-10032) secondary antibodies.

**Sequence Similarity Analysis and Structural Homology Modeling**: Sequence similarity searches for *P. falciparum* homologs to chicken FPPS (Uniprot P08836) were performed by BLASTP analysis as implemented at the Plasmodium Genomics Resource webpage (www.plasmodb.org). Sequence similarity searches using the PPS (PF3D7_0202700) protein sequence as query were carried out using NCBI BLAST[51] (excluding organisms in the phylum Apicomplexa to which *P. falciparum* belongs) and MPI HHpred[52]. A homology model of PPS was generated by the MPI HHpred software using the X-ray crystallographic structural model of *E.*

*coli* OPPS (PDB 3WJK), which was one of the top 10 homology hits by HHpred analysis, as template. Structural models were visualized using PyMol (Schrödinger).

**β-Carotene Extraction and Analysis by Mass Spectrometry:** For determination of beta-carotene levels in parasite-infected versus uninfected erythrocytes, 35 ml of 4% hematocrit *P. falciparum* culture infected at 13-15% parasitemia with the Dd2 PPS aptamer/TetR-DOZI knockdown parasites were collected after 6 days of growth in the presence or absence of 1 µM aTc. Uninfected erythrocyte samples were prepared by collecting 20 ml of 4% hematocrit uninfected culture incubated for 6 days in RPMI media that lacked or contained 2.5 g/L AlbuMAX. Samples of infected or uninfected erythrocytes were harvested by centrifugation, lysed by 0.05% saponin, and pelleted by centrifugation. Saponin pellets were washed in PBS and then extracted three times in 1 ml of chilled acetone (pellet was briefly sonicated after addition of the first acetone volume). The supernatant of each extraction was pooled and dried down by vacuum concentration (Speed Vac). Three biological replicates of each sample were prepared. For analysis of AlbuMAX, 85 mg of dry AlbuMAX (equivalent to the AlbuMAX content in 35 ml of complete culture media) was extracted in 3 volumes of cold acetone, and supernatants were combined and dried as above.

For analysis of β-carotene synthesis, NF54 PfMev parasites were cultured and expanded over three intraerythrocytic cycles in media containing 50 µM 2-$^{13}$C-mevalonate and 10 µM fosmidomycin. This strategy was chosen to inhibit MEP pathway activity, ensure full $^{13}$C-labeling of the endogenous IPP and DMAPP precursor pool within parasites produced by the cytoplasmic bypass enzymes, and result in a distinguishable 8 Da mass increase for any β-carotene derived from de novo synthesis. Final parasite samples contained 70 ml of culture at 15% parasitemia and

were collected by centrifugation prior to 0.05 % saponin lysis, centrifugation, and washing the pellet in PBS. The final pellet was extracted in acetone and dried, as described above.

As a positive control for detecting isotopic incorporation of $^{13}$C-labeled precursors into biosynthesized β-carotene, we turned to studies of *E. coli* bacteria engineered to biosynthesize β-carotene[64] and grown in minimal M9 medium with uniformly labeled $^{13}$C-glucose as the sole carbon source. Growth of bacteria in these conditions was expected to lead to a 40-Da mass increase in detected β-carotene. 5-ml cultures of pAC-BETAipi *E. coli* or untransformed Top10 *E. coli* were allowed to expand over two days at 30˚ C in the dark. Bacterial cultures were harvested by centrifugation at 5,000 rpm for 10 min., and bacterial pellets were extracted three times in cold acetone and dried, as described above.

LC-MS-grade methanol, acetonitrile, isopropyl alcohol, chloroform, and formic acid were purchased from VWR. Samples were resuspended in 50 µl MeOH/$CHCl_3$ (2mM LiI), and a sample volume of 10 µl was injected onto a Phenomenex Luna 150 x 2.1 mm reverse-phase C8 column maintained at 30 °C and connected to an Agilent HiP 1290 Sampler, Agilent 1290 Infinity pump, and Agilent 6545 Accurate Mass Q-TOF dual AJS-ESI mass spectrometer. The instrument was operated in positive ion mode, and the source gas temperature was 275 °C with a drying gas flow of 12 L/min, nebulizer pressure of 35 psig, sheath gas temp of 325 °C and sheath gas flow of 12 L/min. VCap voltage was set at 3500 V, nozzle voltage 250 V, fragmentor at 90 V, skimmer at 65 V, octopole RF peak at 750 V and a scan range *m/z* 40 - 900. The mobile solvent phase A was $H_2O$ with 0.1% formic acid, and mobile phase B was MeOH:ACN:IPA (2:2:1 v/v) with 0.1% formic acid. The chromatography gradient started at 80% mobile phase B then increased to 100% B over 6 min where it was held until 9.9 min and then returned to the initial conditions and equilibrated for 5 min. The column flow rate was 0.5 mL/min.

Results from LC-MS experiments were collected using Agilent Mass Hunter (MH) Workstation and analyzed using the software packages MH Qual and MH Quant (Agilent Technologies, Inc.). Unlabeled, 2-$^{13}$C-mevalonate-labeled, and uniform $^{13}$C-glucose-labeled ß-carotene were analyzed using the molecular ions of *m/z* 536.4377, *m/z* 544.4645, and *m/z* 576.5718, respectively. Fragmentation profiling of unlabeled ß-carotene by MS/MS confirmed the expected product ions at *m/z* 444 and *m/z* 119, as previously reported.[86] For quantitation of unlabeled ß-carotene levels in experimental samples and determination of a limit of detection (LOD), a calibration curve was constructed using serial dilutions of commercial ß-carotene (Sigma C9750). The concentration LOD for a 10-µl sample of unlabeled ß-carotene in this assay was 2.6 ng/mL. Integrated peak areas for unlabeled ß-carotene in experimental samples were converted to concentration values in the 10-µL sample using this calibration curve.

| **Primers used in this study** | | |
|---|---|---|
| **No.** | **Name** | **Sequence (5' to 3')** |
| 1 | PPS-EOE-F | ACACGATTTTTTCTCGAGATGGTTCACCTAAGTAAAAGAAATAATATTAAAAGCTTTTTA |
| 2 | PPS-GFP-TEOE-R | TGCTGCACCTGGCCTAGGTTTGACGTTTCTTGATAACACGTTTAAGATTAAATTAATTAA |
| 3 | PPS-RFP-TyEOE-R | TCAATTAAGTTTCCTAGGTTTGACGTTTCTTGATAACACGTTTAAGATTAAATTAATTAA |
| 4 | SufB-F | ACGATTTTTTCTCGAGATGATAAAATTAAAAAATTTTTTAAATATTTATAATTTAAATTA |
| 5 | SufB-R | TAGACACCATCCTAGGATTAAATATATCTTTAATTTTTAATGAAAATAATATAGGTATCT |
| 6 | PPS-Cas9gRNA1-F | TAAGTATATAATATTCGTGCTAGTTCTATTTTTGCGTTTTAGAGCTAGAA |
| 7 | PPS-Cas9gRNA1-R | TTCTAGCTCTAAAACGCAAAAATAGAACTAGCACGAATATTATATACTTA |
| 8 | PPS-Cas9gRNA2-F | TAAGTATATAATATTGATGATTCAAATAAAAGAAGGTTTTAGAGCTAGAA |
| 9 | PPS-Cas9gRNA2-R | TTCTAGCTCTAAAACCTTCTTTTATTTGAATCATCAATATTATATACTTA |
| 10 | PPS-Cas9gRNA4-F | TAAGTATATAATATT TGATATAAAACAAAGTAGCG GTTTTAGAGCTAGAA |
| 11 | PPS-Cas9gRNA4-R | TTCTAGCTCTAAAACCGCTACTTTGTTTTATATCAAATATTATATACTTA |
| 12 | Cas9HindIII-F | AATATTAAGCTTGTTTTAGAGCTAGAAATAGCAAGTTAAAATAAGGCTAGTCCGTTATCA |
| 13 | Cas9HindIII-R | TAAAACAAGCTTAATATTATATACTTAATATGAAATATGTGCATATAGGAAAAATTATGCA TTTTGGTTACTCTAATATTATATATATAT |
| 14 | PPS_3'UTR_HF-F | GGCCCCTTTCCGGGCGCGCCCAATAACATATACAATATCAAACATATATATTATAATATTA TTAAACATCTTCAATATTGTATTATTTAA |
| 15 | PPS_3'UTR_HF-R | TAATGCTATGACACCTCTTCTTTTATTTGACTTAAGTATGTTTGATACATGTAGATTTCTTA AAGAATGAAGCTTA |
| 16 | PPS_3'CR_HF-F | TTTAAGAAATCTACATGTATCAAACATACTTAAGTCAAATAAAAGAAGAGGTGTCATAGC |
| 17 | PPS_3'CR_HF-R | GTCATAAGGATAGACGTCATCATTTGACGTTTCTTGATAACACG |
| 18 | PPS_3'CR_HF-SM-R | CATAAGGATAGACGTCTTTGACGTTTCTTGATAACACGTTTAAGATTAAATTAATTAATGC TTCGCTACTTTGTTTTATATCATCATGTT |
| 19 | miaA.HA1.F | GCCACGAGCGGCCGTAAATTAAAGACAACGGGCTGTCAAC |
| 20 | miaA.HA1.R | AAGCGCAGCGGCCGGGAATTTCCATCTCTAAAAAAGTTCA |
| 21 | miaA.HA2.F | CGACAGACGCCGGTGAAAGAAATGATGATATGGTAGAATT |
| 22 | miaA.HA2.R | GGCCACCAGCCGGCGATATCCATCTTCTTTGTTTCTTGGC |
| 23 | miaA.gRNA.F | TAAGTATATAATATTAATAACGATATTAAATGTAAGTTTTAGAGCTAGAA |
| 24 | miaA.gRNA.R | TTCTAGCTCTAAAACTTACATTTAATATCGTTATTAATATTATATACTTA |

| | | |
|---|---|---|
| 25 | miaA.5.F | GTTGAATAAATAAATGCCTCTCTATATATTGTTAACAT |
| 26 | miaA.5.WT.R | CTTCGACTTTAGCAATACCTACATTG |
| 27 | miaA.3.F | GGGAATCAGTAATTGATATAAGAAAAGAAG |
| 28 | miaA.3.WT.R | AAACTTCAAGACAATGCCTATAGC |
| 29 | pRS.F | CATATTTATTAAATCTAGAATTCGACAGACGCCGG |
| 30 | pRS.R | TACAAAATGCTTAAGCGCAGCGGCC |
| 31 | I5P-qPCR-F | GACATAAGTTTAGTAGGTCG |
| 32 | I5P-qPCR-R | TTCTGACTCCACATCATTTG |
| 33 | ADSL-qPCR-F | GGAAATCCATAGACAAACAATG |
| 34 | ADSL-qPCR-R | TCCTGTGAGAAGTGCTCCAC |
| 35 | TufA-qPCR-F | AAGATGTATTTTCTATAACAGGTAGAGGTA |
| 36 | TufA-qPCR-R | AACTGTTGTTAAATTAGGAGATGATTTTTC |
| 37 | PPS-qPCR-F | ATCAGGGGATTATCTCTTAGCAC |
| 38 | PPS-qPCR-R | AACTTTCGACAACATAAGAGAAACT |
| 39 | 3'APT-F | CTTATGACGTACCTGATTATGCAC |
| 40 | 10x APT-R | GTAGACCCCATTGTGAGTACATAAATATATTATATAAACTAGACTAGG |

**ACKNOWLEDGEMENTS:** We thank Belén Cassera, James Cox, Dale Poulter and members of the Sigala lab for helpful discussions. Research reported in this publication was supported by Department of Defense PRMRP Discovery Award W81XWH1810060 (to PAS), National Institutes of Health grants R35GM133764 (to PAS) and AI125534 (to STP), a Burroughs Wellcome Fund Career Award at the Scientific Interface (to PAS), the Johns Hopkins Malaria Research Institute (STP), and the Bloomberg Family Foundation (STP). PAS is a Pew Scholar in the Biomedical Sciences, supported by The Pew Charitable Trusts. MO and KR were supported in part by NIH training grants T32DK007115 and T32AI007417, respectively. Metabolomics analyses were supported in part by NIH grant U54DK110858. DNA synthesis and sequencing, epifluorescence microscopy, mass spectrometry metabolomics, generation of CRISPR/Cas9 reagents, and flow cytometry were performed using core facilities at the University of Utah. Mass spectrometry equipment was obtained through NCRR Shared Instrumentation Grants 1S10OD016232-01, 1S10OD018210-01A1 and 1S10OD021505-01.

# REFERENCES

[1] Ralph, S. A., van Dooren, G. G., Waller, R. F., Crawford, M. J., Fraunholz, M. J., Foth, B. J., Tonkin, C. J., Roos, D. S., and McFadden, G. I. (2004) Metabolic maps and functions of the Plasmodium falciparum apicoplast, *Nat. Rev. Microbiol. 2*, 203-216.

[2] Ke, H., Sigala, P. A., Miura, K., Morrisey, J. M., Mather, M. W., Crowley, J. R., Henderson, J. P., Goldberg, D. E., Long, C. A., and Vaidya, A. B. (2014) The heme biosynthesis pathway is essential for Plasmodium falciparum development in mosquito stage but not in blood stages, *J. Biol. Chem. 289*, 34827-34837. DOI: https://doi.org/10.1074/jbc.M114.615831

[3] Goldberg, D. E., and Sigala, P. A. (2017) Plasmodium heme biosynthesis: To be or not to be essential?, *PLoS Pathog. 13*, e1006511. DOI: https://doi.org/10.1371/journal.ppat.1006511

[4] Yu, M., Kumar, T. R. S., Nkrumah, L. J., Coppi, A., Retzlaff, S., Li, C. D., Kelly, B. J., Moura, P. A., Lakshmanan, V., Freundlich, J. S., Valderramos, J. C., Vilcheze, C., Siedner, M., Tsai, J. H. C., Falkard, B., Sidhu, A. B. S., Purcell, L. A., Gratraud, P., Kremer, L., Waters, A. P., Schiehser, G., Jacobus, D. P., Janse, C. J., Ager, A., Jacobs, W. R., Sacchettini, J. C., Heussler, V., Sinni, P., and Fidock, D. A. (2008) The Fatty Acid Biosynthesis Enzyme FabI Plays a Key Role in the Development of Liver-Stage Malarial Parasites, *Cell Host Microbe 4*, 567-578. DOI: https://doi.org/10.1016/J.Chom.2008.11.001

[5] Shears, M. J., Botte, C. Y., and McFadden, G. I. (2015) Fatty acid metabolism in the Plasmodium apicoplast: Drugs, doubts and knockouts, *Mol. Biochem. Parasitol. 199*, 34-50. DOI: https://doi.org/10.1016/j.molbiopara.2015.03.004

[6] Dahl, E. L., and Rosenthal, P. J. (2007) Multiple antibiotics exert delayed effects against the Plasmodium falciparum apicoplast, *Antimicrob. Agents Chemother. 51*, 3485-3490. DOI: https://doi.org/10.1128/AAC.00527-07

[7] Guggisberg, A. M., Amthor, R. E., and Odom, A. R. (2014) Isoprenoid biosynthesis in Plasmodium falciparum, *Eukaryot. Cell 13*, 1348-1359. DOI: https://doi.org/10.1128/EC.00160-14

[8] Jomaa, H., Wiesner, J., Sanderbrand, S., Altincicek, B., Weidemeyer, C., Hintz, M., Turbachova, I., Eberl, M., Zeidler, J., Lichtenthaler, H. K., Soldati, D., and Beck, E. (1999) Inhibitors of the nonmevalonate pathway of isoprenoid biosynthesis as antimalarial drugs, *Science 285*, 1573-1576. DOI: https://doi.org/10.1126/science.285.5433.1573

[9] van Dooren, G. G., Stimmler, L. M., and McFadden, G. I. (2006) Metabolic maps and functions of the Plasmodium mitochondrion, *FEMS Microbiol. Rev. 30*, 596-630. DOI: https://doi.org/10.1111/j.1574-6976.2006.00027.x

[10] Simao-Gurge, R. M., Wunderlich, G., Cricco, J. A., Cubillos, E. F. G., Domenech-Carbo, A., Cebrian-Torrejon, G., Almeida, F. G., Cirulli, B. A., and Katzin, A. M. (2019) Biosynthesis of heme O in intraerythrocytic stages of Plasmodium falciparum and potential inhibitors of this pathway, *Sci. Rep. 9*, 19261. DOI: https://doi.org/10.1038/s41598-019-55506-y

[11] Yeh, E., and DeRisi, J. L. (2011) Chemical rescue of malaria parasites lacking an apicoplast defines organelle function in blood-stage Plasmodium falciparum, *PLoS Biol. 9*, e1001138. DOI: https://doi.org/10.1371/journal.pbio.1001138

[12] Uddin, T., McFadden, G. I., and Goodman, C. D. (2018) Validation of Putative Apicoplast-Targeting Drugs Using a Chemical Supplementation Assay in Cultured Human Malaria Parasites, *Antimicrob. Agents Chemother. 62*. DOI: https://doi.org/10.1128/AAC.01161-17

[13] Ramya, T. N., Mishra, S., Karmodiya, K., Surolia, N., and Surolia, A. (2007) Inhibitors of nonhousekeeping functions of the apicoplast defy delayed death in Plasmodium falciparum, *Antimicrob. Agents Chemother. 51*, 307-316. DOI: https://doi.org/10.1128/AAC.00808-06

[14] Kennedy, K., Crisafulli, E. M., and Ralph, S. A. (2019) Delayed Death by Plastid Inhibition in Apicomplexan Parasites, *Trends Parasitol. 35*, 747-759. DOI: https://doi.org/10.1016/j.pt.2019.07.010

[15] Kennedy, K., Cobbold, S. A., Hanssen, E., Birnbaum, J., Spillman, N. J., McHugh, E., Brown, H., Tilley, L., Spielmann, T., McConville, M. J., and Ralph, S. A. (2019) Delayed death in the malaria parasite Plasmodium falciparum is caused by disruption of prenylation-dependent intracellular trafficking, *PLoS Biol. 17*, e3000376. DOI: https://doi.org/10.1371/journal.pbio.3000376

[16] Amberg-Johnson, K., Hari, S. B., Ganesan, S. M., Lorenzi, H. A., Sauer, R. T., Niles, J. C., and Yeh, E. (2017) Small molecule inhibition of apicomplexan FtsH1 disrupts plastid biogenesis in human pathogens, *Elife 6*. DOI: https://doi.org/10.7554/eLife.29865

[17] Boucher, M. J., and Yeh, E. (2019) Disruption of Apicoplast Biogenesis by Chemical Stabilization of an Imported Protein Evades the Delayed-Death Phenotype in Malaria Parasites, *mSphere 4*. DOI: https://doi.org/10.1128/mSphere.00710-18

[18] Okada, M., Guo, P., Nalder, S. A., and Sigala, P. A. (2020) Doxycycline has distinct apicoplast-specific mechanisms of antimalarial activity, *Elife 9*. DOI: https://doi.org/10.7554/eLife.60246

[19] Gisselberg, J. E., Herrera, Z., Orchard, L. M., Llinas, M., and Yeh, E. (2018) Specific Inhibition of the Bifunctional Farnesyl/Geranylgeranyl Diphosphate Synthase in Malaria Parasites via a New Small-Molecule Binding Site, *Cell Chem. Biol. 25*, 185-193 e185. DOI: https://doi.org/10.1016/j.chembiol.2017.11.010

[20] Imlay, L., and Odom, A. R. (2014) Isoprenoid metabolism in apicomplexan parasites, *Curr. Clin. Microbiol. Rep. 1*, 37-50. DOI: https://doi.org/10.1007/s40588-014-0006-7

[21] Gisselberg, J. E., Dellibovi-Ragheb, T. A., Matthews, K. A., Bosch, G., and Prigge, S. T. (2013) The suf iron-sulfur cluster synthesis pathway is required for apicoplast maintenance in malaria parasites, *PLoS Pathog. 9*, e1003655. DOI: https://doi.org/10.1371/journal.ppat.1003655

[22] Gabriel, H. B., de Azevedo, M. F., Palmisano, G., Wunderlich, G., Kimura, E. A., Katzin, A. M., and Alves, J. M. (2015) Single-target high-throughput transcription analyses reveal high levels of alternative splicing present in the FPPS/GGPPS from Plasmodium falciparum, *Sci. Rep. 5*, 18429. DOI: https://doi.org/10.1038/srep18429

[23] No, J. H., de Macedo Dossin, F., Zhang, Y., Liu, Y. L., Zhu, W., Feng, X., Yoo, J. A., Lee, E., Wang, K., Hui, R., Freitas-Junior, L. H., and Oldfield, E. (2012) Lipophilic analogs of zoledronate and risedronate inhibit Plasmodium geranylgeranyl diphosphate synthase (GGPPS) and exhibit potent antimalarial activity, *Proc. Natl. Acad. Sci. U. S. A. 109*, 4058-4063. DOI: https://doi.org/10.1073/pnas.1118215109

[24] Tonhosolo, R., D'Alexandri, F. L., Genta, F. A., Wunderlich, G., Gozzo, F. C., Eberlin, M. N., Peres, V. J., Kimura, E. A., and Katzin, A. M. (2005) Identification, molecular

cloning and functional characterization of an octaprenyl pyrophosphate synthase in intra-erythrocytic stages of Plasmodium falciparum, *Biochem. J. 392*, 117-126. DOI: https://doi.org/10.1042/BJ20050441

[25] Nair, S. C., Brooks, C. F., Goodman, C. D., Sturm, A., McFadden, G. I., Sundriyal, S., Anglin, J. L., Song, Y., Moreno, S. N., and Striepen, B. (2011) Apicoplast isoprenoid precursor synthesis and the molecular basis of fosmidomycin resistance in Toxoplasma gondii, *J. Exp. Med. 208*, 1547-1559. DOI: https://doi.org/10.1084/jem.20110039

[26] Bowman, J. D., Merino, E. F., Brooks, C. F., Striepen, B., Carlier, P. R., and Cassera, M. B. (2014) Antiapicoplast and gametocytocidal screening to identify the mechanisms of action of compounds within the malaria box, *Antimicrob. Agents Chemother. 58*, 811-819. DOI: https://doi.org/10.1128/AAC.01500-13

[27] Goodman, C. D., and McFadden, G. I. (2014) Ycf93 (Orf105), a small apicoplast-encoded membrane protein in the relict plastid of the malaria parasite Plasmodium falciparum that is conserved in Apicomplexa, *PLoS One 9*, e91178. DOI: https://doi.org/10.1371/journal.pone.0091178

[28] Waller, R. F., Reed, M. B., Cowman, A. F., and McFadden, G. I. (2000) Protein trafficking to the plastid of *Plasmodium falciparum* is via the secretory pathway, *EMBO J. 19*, 1794-1802.

[29] Swift, R. P., Rajaram, K., Liu, H. B., Dziedzic, A., Jedlicka, A. E., Roberts, A. D., Matthews, K. A., Jhun, H., Bumpus, N. N., Tewari, S. G., Wallqvist, A., and Prigge, S. T. (2020) A mevalonate bypass system facilitates elucidation of plastid biology in malaria parasites, *PLoS Pathog. 16*, e1008316. DOI: https://doi.org/10.1371/journal.ppat.1008316

[30] Howe, R., Kelly, M., Jimah, J., Hodge, D., and Odom, A. R. (2013) Isoprenoid biosynthesis inhibition disrupts Rab5 localization and food vacuolar integrity in Plasmodium falciparum, *Eukaryot. Cell 12*, 215-223. DOI: https://doi.org/10.1128/EC.00073-12

[31] Zhang, B., Watts, K. M., Hodge, D., Kemp, L. M., Hunstad, D. A., Hicks, L. M., and Odom, A. R. (2011) A second target of the antimalarial and antibacterial agent fosmidomycin revealed by cellular metabolic profiling, *Biochemistry 50*, 3570-3577. DOI: https://doi.org/10.1021/bi200113y

[32] Cassera, M. B., Gozzo, F. C., D'Alexandri, F. L., Merino, E. F., del Portillo, H. A., Peres, V. J., Almeida, I. C., Eberlin, M. N., Wunderlich, G., Wiesner, J., Jomaa, H., Kimura, E. A., and Katzin, A. M. (2004) The methylerythritol phosphate pathway is functionally active in all intraerythrocytic stages of Plasmodium falciparum, *J. Biol. Chem. 279*, 51749-51759. DOI: https://doi.org/10.1074/jbc.M408360200

[33] Phillips, M. A., Gujjar, R., Malmquist, N. A., White, J., El Mazouni, F., Baldwin, J., and Rathod, P. K. (2008) Triazolopyrimidine-based dihydroorotate dehydrogenase inhibitors with potent and selective activity against the malaria parasite Plasmodium falciparum, *J. Med. Chem. 51*, 3649-3653. DOI: https://doi.org/10.1021/jm8001026

[34] Fry, M., and Pudney, M. (1992) Site of action of the antimalarial hydroxynaphthoquinone, 2-[trans-4-(4'-chlorophenyl) cyclohexyl]-3-hydroxy-1,4-naphthoquinone (566C80), *Biochem. Pharmacol. 43*, 1545-1553. DOI: https://doi.org/10.1016/0006-2952(92)90213-3

[35] Mamoun, C. B., Gluzman, I. Y., Goyard, S., Beverley, S. M., and Goldberg, D. E. (1999) A set of independent selectable markers for transfection of the human malaria parasite

Plasmodium falciparum, *Proc. Natl. Acad. Sci. U. S. A. 96*, 8716-8720. DOI: https://doi.org/10.1073/pnas.96.15.8716

[36] Fidock, D. A., and Wellems, T. E. (1997) Transformation with human dihydrofolate reductase renders malaria parasites insensitive to WR99210 but does not affect the intrinsic activity of proguanil, *Proc. Natl. Acad. Sci. U. S. A. 94*, 10931-10936. DOI: https://doi.org/10.1073/pnas.94.20.10931

[37] Swift, R. P., Rajaram, K., Keutcha, C., Liu, H. B., Kwan, B., Dziedzic, A., Jedlicka, A. E., and Prigge, S. T. (2020) The NTP generating activity of pyruvate kinase II is critical for apicoplast maintenance in Plasmodium falciparum, *Elife 9*. DOI: https://doi.org/10.7554/eLife.50807

[38] Dahl, E. L., Shock, J. L., Shenai, B. R., Gut, J., DeRisi, J. L., and Rosenthal, P. J. (2006) Tetracyclines specifically target the apicoplast of the malaria parasite Plasmodium falciparum, *Antimicrob. Agents Chemother. 50*, 3124-3131. DOI: https://doi.org/10.1128/AAC.00394-06

[39] van Dooren, G. G., Marti, M., Tonkin, C. J., Stimmler, L. M., Cowman, A. F., and McFadden, G. I. (2005) Development of the endoplasmic reticulum, mitochondrion and apicoplast during the asexual life cycle of Plasmodium falciparum, *Mol. Microbiol. 57*, 405-419. DOI: https://doi.org/10.1111/j.1365-2958.2005.04699.x

[40] Persson, B. C., Esberg, B., Olafsson, O., and Bjork, G. R. (1994) Synthesis and function of isopentenyl adenosine derivatives in tRNA, *Biochimie 76*, 1152-1160. DOI: https://doi.org/10.1016/0300-9084(94)90044-2

[41] Esberg, B., Leung, H. C., Tsui, H. C., Bjork, G. R., and Winkler, M. E. (1999) Identification of the miaB gene, involved in methylthiolation of isopentenylated A37 derivatives in the tRNA of Salmonella typhimurium and Escherichia coli, *J. Bacteriol. 181*, 7256-7265. DOI: https://doi.org/10.1128/JB.181.23.7256-7265.1999

[42] Boucher, M. J., Ghosh, S., Zhang, L., Lal, A., Jang, S. W., Ju, A., Zhang, S., Wang, X., Ralph, S. A., Zou, J., Elias, J. E., and Yeh, E. (2018) Integrative proteomics and bioinformatic prediction enable a high-confidence apicoplast proteome in malaria parasites, *PLoS Biol. 16*, e2005895. DOI: https://doi.org/10.1371/journal.pbio.2005895

[43] Bushell, E., Gomes, A. R., Sanderson, T., Anar, B., Girling, G., Herd, C., Metcalf, T., Modrzynska, K., Schwach, F., Martin, R. E., Mather, M. W., McFadden, G. I., Parts, L., Rutledge, G. G., Vaidya, A. B., Wengelnik, K., Rayner, J. C., and Billker, O. (2017) Functional Profiling of a Plasmodium Genome Reveals an Abundance of Essential Genes, *Cell 170*, 260-272 e268. DOI: https://doi.org/10.1016/j.cell.2017.06.030

[44] Zhang, M., Wang, C., Otto, T. D., Oberstaller, J., Liao, X., Adapa, S. R., Udenze, K., Bronner, I. F., Casandra, D., Mayho, M., Brown, J., Li, S., Swanson, J., Rayner, J. C., Jiang, R. H. Y., and Adams, J. H. (2018) Uncovering the essential genes of the human malaria parasite Plasmodium falciparum by saturation mutagenesis, *Science 360*. DOI: https://doi.org/10.1126/science.aap7847

[45] Kellogg, B. A., and Poulter, C. D. (1997) Chain elongation in the isoprenoid biosynthetic pathway, *Curr. Opin. Chem. Biol. 1*, 570-578. DOI: https://doi.org/10.1016/s1367-5931(97)80054-3

[46] Poulter, C. D. (2006) Farnesyl diphosphate synthase. A paradigm for understanding structure and functional relationships in E-polyprenyl diphosphate synthases, *Phytochem. Rev. 5*, 17-26. DOI: https://doi.org/10.1007/s11101-005-4887-1

[47] Thulasiram, H. V., and Poulter, C. D. (2006) Farnesyl diphosphate synthase: The art of compromise between substrate selectivity and stereoselectivity, *J. Am. Chem. Soc. 128*, 15819-15823. DOI: https://doi.org/10.1021/ja065573b

[48] Tarshis, L. C., Proteau, P. J., Kellogg, B. A., Sacchettini, J. C., and Poulter, C. D. (1996) Regulation of product chain length by isoprenyl diphosphate synthases, *Proc. Natl. Acad. Sci. U. S. A. 93*, 15018-15023. DOI: https://doi.org/10.1073/pnas.93.26.15018

[49] Jordao, F. M., Gabriel, H. B., Alves, J. M., Angeli, C. B., Bifano, T. D., Breda, A., de Azevedo, M. F., Basso, L. A., Wunderlich, G., Kimura, E. A., and Katzin, A. M. (2013) Cloning and characterization of bifunctional enzyme farnesyl diphosphate/geranylgeranyl diphosphate synthase from Plasmodium falciparum, *Malar. J. 12*, 184. DOI: https://doi.org/10.1186/1475-2875-12-184

[50] Artz, J. D., Wernimont, A. K., Dunford, J. E., Schapira, M., Dong, A., Zhao, Y., Lew, J., Russell, R. G., Ebetino, F. H., Oppermann, U., and Hui, R. (2011) Molecular characterization of a novel geranylgeranyl pyrophosphate synthase from Plasmodium parasites, *J. Biol. Chem. 286*, 3315-3322. DOI: https://doi.org/10.1074/jbc.M109.027235

[51] Boratyn, G. M., Camacho, C., Cooper, P. S., Coulouris, G., Fong, A., Ma, N., Madden, T. L., Matten, W. T., McGinnis, S. D., Merezhuk, Y., Raytselis, Y., Sayers, E. W., Tao, T., Ye, J., and Zaretskaya, I. (2013) BLAST: a more efficient report with usability improvements, *Nucleic Acids Res. 41*, W29-33. DOI: https://doi.org/10.1093/nar/gkt282

[52] Zimmermann, L., Stephens, A., Nam, S. Z., Rau, D., Kubler, J., Lozajic, M., Gabler, F., Soding, J., Lupas, A. N., and Alva, V. (2018) A Completely Reimplemented MPI Bioinformatics Toolkit with a New HHpred Server at its Core, *J. Mol. Biol. 430*, 2237-2243. DOI: https://doi.org/10.1016/j.jmb.2017.12.007

[53] Tonhosolo, R., D'Alexandri, F. L., de Rosso, V. V., Gazarini, M. L., Matsumura, M. Y., Peres, V. J., Merino, E. F., Carlton, J. M., Wunderlich, G., Mercadante, A. Z., Kimura, E. A., and Katzin, A. M. (2009) Carotenoid biosynthesis in intraerythrocytic stages of Plasmodium falciparum, *J. Biol. Chem. 284*, 9974-9985. DOI: https://doi.org/10.1074/jbc.M807464200

[54] Foth, B. J., Ralph, S. A., Tonkin, C. J., Struck, N. S., Fraunholz, M., Roos, D. S., Cowman, A. F., and McFadden, G. I. (2003) Dissecting apicoplast targeting in the malaria parasite Plasmodium falciparum, *Science 299*, 705-708.

[55] Sigala, P. A., Crowley, J. R., Henderson, J. P., and Goldberg, D. E. (2015) Deconvoluting heme biosynthesis to target blood-stage malaria parasites, *Elife 4*. DOI: https://doi.org/10.7554/eLife.09143

[56] Ghorbal, M., Gorman, M., Macpherson, C. R., Martins, R. M., Scherf, A., and Lopez-Rubio, J. J. (2014) Genome editing in the human malaria parasite Plasmodium falciparum using the CRISPR-Cas9 system, *Nat. Biotechnol. 32*, 819-821. DOI: https://doi.org/10.1038/nbt.2925

[57] Ganesan, S. M., Falla, A., Goldfless, S. J., Nasamu, A. S., and Niles, J. C. (2016) Synthetic RNA-protein modules integrated with native translation mechanisms to control gene expression in malaria parasites, *Nat. Commun. 7*, 10727. DOI: https://doi.org/10.1038/ncomms10727

[58] Maruthi, M., Ling, L., Zhou, J., and Ke, H. (2020) Dispensable Role of Mitochondrial Fission Protein 1 (Fis1) in the Erythrocytic Development of Plasmodium falciparum, *mSphere 5*. DOI: https://doi.org/10.1128/mSphere.00579-20

[59] Gabriel, H. B., Silva, M. F., Kimura, E. A., Wunderlich, G., Katzin, A. M., and Azevedo, M. F. (2015) Squalestatin is an inhibitor of carotenoid biosynthesis in Plasmodium falciparum, *Antimicrob. Agents Chemother. 59*, 3180-3188. DOI: https://doi.org/10.1128/AAC.04500-14

[60] Bouvier, F., Rahier, A., and Camara, B. (2005) Biogenesis, molecular regulation and function of plant isoprenoids, *Prog. Lipid Res. 44*, 357-429. DOI: https://doi.org/10.1016/j.plipres.2005.09.003

[61] Zhou, X., Welsch, R., Yang, Y., Alvarez, D., Riediger, M., Yuan, H., Fish, T., Liu, J., Thannhauser, T. W., and Li, L. (2015) Arabidopsis OR proteins are the major posttranscriptional regulators of phytoene synthase in controlling carotenoid biosynthesis, *Proc. Natl. Acad. Sci. U. S. A. 112*, 3558-3563. DOI: https://doi.org/10.1073/pnas.1420831112

[62] Iwata-Reuyl, D., Math, S. K., Desai, S. B., and Poulter, C. D. (2003) Bacterial phytoene synthase: molecular cloning, expression, and characterization of Erwinia herbicola phytoene synthase, *Biochemistry 42*, 3359-3365. DOI: https://doi.org/10.1021/bi0206614

[63] Nagashima, S., Kamimura, A., Shimizu, T., Nakamura-Isaki, S., Aono, E., Sakamoto, K., Ichikawa, N., Nakazawa, H., Sekine, M., Yamazaki, S., Fujita, N., Shimada, K., Hanada, S., and Nagashima, K. V. (2012) Complete genome sequence of phototrophic betaproteobacterium Rubrivivax gelatinosus IL144, *J. Bacteriol. 194*, 3541-3542. DOI: https://doi.org/10.1128/JB.00511-12

[64] Cunningham, F. X., Jr., and Gantt, E. (2005) A study in scarlet: enzymes of ketocarotenoid biosynthesis in the flowers of Adonis aestivalis, *Plant J. 41*, 478-492. DOI: https://doi.org/10.1111/j.1365-313X.2004.02309.x

[65] McFadden, G. I., and Yeh, E. (2016) The apicoplast: now you see it, now you don't, *Int. J. Parasitol.* DOI: https://doi.org/10.1016/j.ijpara.2016.08.005

[66] Akhtar, T. A., Surowiecki, P., Siekierska, H., Kania, M., Van Gelder, K., Rea, K. A., Virta, L. K. A., Vatta, M., Gawarecka, K., Wojcik, J., Danikiewicz, W., Buszewicz, D., Swiezewska, E., and Surmacz, L. (2017) Polyprenols Are Synthesized by a Plastidial cis-Prenyltransferase and Influence Photosynthetic Performance, *Plant Cell 29*, 1709-1725. DOI: https://doi.org/10.1105/tpc.16.00796

[67] Joyard, J., Ferro, M., Masselon, C., Seigneurin-Berny, D., Salvi, D., Garin, J., and Rolland, N. (2009) Chloroplast proteomics and the compartmentation of plastidial isoprenoid biosynthetic pathways, *Mol. Plant 2*, 1154-1180. DOI: https://doi.org/10.1093/mp/ssp088

[68] Van Gelder, K., Rea, K. A., Virta, L. K. A., Whitnell, K. L., Osborn, M., Vatta, M., Khozin, A., Skorupinska-Tudek, K., Surmacz, L., and Akhtar, T. A. (2018) Medium-Chain Polyprenols Influence Chloroplast Membrane Dynamics in Solanum lycopersicum, *Plant Cell Physiol. 59*, 2350-2365. DOI: https://doi.org/10.1093/pcp/pcy157

[69] Kelly, M., Su, C. Y., Schaber, C., Crowley, J. R., Hsu, F. F., Carlson, J. R., and Odom, A. R. (2015) Malaria parasites produce volatile mosquito attractants, *mBio 6*. DOI: https://doi.org/10.1128/mBio.00235-15

[70] Emami, S. N., Lindberg, B. G., Hua, S., Hill, S. R., Mozuraitis, R., Lehmann, P., Birgersson, G., Borg-Karlson, A. K., Ignell, R., and Faye, I. (2017) A key malaria metabolite modulates vector blood seeking, feeding, and susceptibility to infection, *Science 355*, 1076-1080. DOI: https://doi.org/10.1126/science.aah4563

[71] Miller, J. J., and Odom John, A. R. (2020) The Malaria Metabolite HMBPP Does Not Trigger Erythrocyte Terpene Release, *ACS Infect. Dis. 6*, 2567-2572. DOI: https://doi.org/10.1021/acsinfecdis.0c00548

[72] Couto, A. S., Kimura, E. A., Peres, V. J., Uhrig, M. L., and Katzin, A. M. (1999) Active isoprenoid pathway in the intra-erythrocytic stages of Plasmodium falciparum: presence of dolichols of 11 and 12 isoprene units, *Biochem. J. 341 ( Pt 3)*, 629-637.

[73] Zimbres, F. M., Valenciano, A. L., Merino, E. F., Florentin, A., Holderman, N. R., He, G., Gawarecka, K., Skorupinska-Tudek, K., Fernandez-Murga, M. L., Swiezewska, E., Wang, X., Muralidharan, V., and Cassera, M. B. (2020) Metabolomics profiling reveals new aspects of dolichol biosynthesis in Plasmodium falciparum, *Sci. Rep. 10*, 13264. DOI: https://doi.org/10.1038/s41598-020-70246-0

[74] Hartley, M. D., and Imperiali, B. (2012) At the membrane frontier: a prospectus on the remarkable evolutionary conservation of polyprenols and polyprenyl-phosphates, *Arch. Biochem. Biophys. 517*, 83-97. DOI: https://doi.org/10.1016/j.abb.2011.10.018

[75] Swiezewska, E., and Danikiewicz, W. (2005) Polyisoprenoids: structure, biosynthesis and function, *Prog. Lipid Res. 44*, 235-258. DOI: https://doi.org/10.1016/j.plipres.2005.05.002

[76] Botte, C. Y., Yamaryo-Botte, Y., Rupasinghe, T. W., Mullin, K. A., MacRae, J. I., Spurck, T. P., Kalanon, M., Shears, M. J., Coppel, R. L., Crellin, P. K., Marechal, E., McConville, M. J., and McFadden, G. I. (2013) Atypical lipid composition in the purified relict plastid (apicoplast) of malaria parasites, *Proc. Natl. Acad. Sci. U. S. A. 110*, 7506-7511. DOI: https://doi.org/10.1073/pnas.1301251110

[77] Tonkin, C. J., van Dooren, G. G., Spurck, T. P., Struck, N. S., Good, R. T., Handman, E., Cowman, A. F., and McFadden, G. I. (2004) Localization of organellar proteins in *Plasmodium falciparum* using a novel set of transfection vectors and a new immunofluorescence fixation method, *Mol. Biochem. Parasitol. 137*, 13-21.

[78] Gallagher, J. R., and Prigge, S. T. (2010) Plasmodium falciparum acyl carrier protein crystal structures in disulfide-linked and reduced states and their prevalence during blood stage growth, *Proteins 78*, 575-588. DOI: https://doi.org/10.1002/prot.22582

[79] Ganesan, S. M., Morrisey, J. M., Ke, H., Painter, H. J., Laroiya, K., Phillips, M. A., Rathod, P. K., Mather, M. W., and Vaidya, A. B. (2011) Yeast dihydroorotate dehydrogenase as a new selectable marker for *Plasmodium falciparum* transfection, *Mol. Biochem. Parasitol. 177*, 29-34.

[80] Klemba, M., Beatty, W., Gluzman, I., and Goldberg, D. E. (2004) Trafficking of plasmepsin II to the food vacuole of the malaria parasite *Plasmodium falciparum*, *J. Cell Biol. 164*, 47-56.

[81] Beck, J. R., Muralidharan, V., Oksman, A., and Goldberg, D. E. (2014) PTEX component HSP101 mediates export of diverse malaria effectors into host erythrocytes, *Nature 511*, 592-595. DOI: https://doi.org/10.1038/nature13574

[82] Balu, B., Shoue, D. A., Fraser, M. J., and Adams, J. H. (2005) High-efficiency transformation of Plasmodium falciparum by the lepidopteran transposable element piggyBac, *Proc. Natl. Acad. Sci. U. S. A. 102*, 16391-16396. DOI: https://doi.org/Doi 10.1073/Pnas.0504679102

[83] Spillman, N. J., Beck, J. R., Ganesan, S. M., Niles, J. C., and Goldberg, D. E. (2017) The chaperonin TRiC forms an oligomeric complex in the malaria parasite cytosol, *Cell Microbiol. 19*. DOI: https://doi.org/10.1111/cmi.12719

[84] Schmittgen, T. D., and Livak, K. J. (2008) Analyzing real-time PCR data by the comparative C(T) method, *Nat. Protoc. 3*, 1101-1108. DOI: https://doi.org/10.1038/nprot.2008.73

[85] Rajaram, K., Liu, H. B., and Prigge, S. T. (2020) Redesigned TetR-Aptamer System To Control Gene Expression in Plasmodium falciparum, *mSphere 5*. DOI: https://doi.org/10.1128/mSphere.00457-20

[86] Rivera, S. M., Christou, P., and Canela-Garayoa, R. (2014) Identification of carotenoids using mass spectrometry, *Mass Spectrom. Rev. 33*, 353-372. DOI: https://doi.org/10.1002/mas.21390